TARGET TRACKING USING NETWORKS OF COOPERATIVE AGENTS SUBJECT TO
INTERMITTENT SENSING

By

CHRISTIAN G. HARRIS

A THESIS PRESENTED TO THE GRADUATE SCHOOL
OF THE UNIVERSITY OF FLORIDA IN PARTIAL FULFILLMENT
OF THE REQUIREMENTS FOR THE DEGREE OF
MASTER OF SCIENCE

UNIVERSITY OF FLORIDA

2020

To my mother Rosalina Delgado, and my brothers

ACKNOWLEDGMENTS

TABLE OF CONTENTS

LIST OF FIGURES

Abstract of Thesis Presented to the Graduate School
of the University of Florida in Partial Fulfillment of the
Requirements for the Degree of Master of Science

TARGET TRACKING USING NETWORKS OF COOPERATIVE AGENTS SUBJECT TO
INTERMITTENT SENSING

By

Christian G. Harris

August 2020

Chair: Warren E. Dixon
Major: Mechanical Engineering

Using networks of cooperative agents, target tracking solutions are developed
for scenarios where continuous feedback of a target is not available, while providing
performance guarantees for the target tracking objectives. By considering stationary
and mobile networks of cooperative agents (i.e., cameras), the underlying estimator and
predictor framework developed in this thesis is demonstrated to be adaptable to a wide
range of target tracking scenarios.

First, an observer and predictor framework is developed for tracking a moving object
using a sparsely distributed network of stationary cameras. The sparsity of the camera
network is representative of complex environments where continuous image feedback
is not available, which occurs when the target is transitioning between fields-of-view in
the camera network or the target is occluded by objects in the scene. Using a Lyapunov-
based switched systems approach, estimates of the object's pose and motion model are
proven to remain bounded, provided the current network configuration satisfies certain
dwell-time conditions (i.e., minimum time the object needs to be observed and maximum
time the object may remain outside a feedback region). This approach allows for areas
of the network that may cause instabilities in the pose estimates, based on the dwell-
time conditions, to be identified ahead of time and offers insight into how the network
configuration could be augmented to ensure stability of the target's pose estimates.

Second, a controller, estimator, and predictor framework is developed for tracking a moving target using a network of mobile cameras, with non-overlapping fields-of-views and operating regions. Using a Lyapunov-based switched systems approach, the proposed framework is proven to be robust to intermittent feedback, and estimates of the target's pose and motion model are proven to remain bounded, provided that minimum and maximum dwell-time conditions are satisfied (i.e., minimum time the target must be observed and maximum time the target may be unobserved, respectively). This framework allows for teams of cooperative agents to track a moving target in complex environments, while increasing the effective target tracking area and guaranteeing tracking performance.

CHAPTER 1
INTRODUCTION

Advances in computer vision and imaging technologies have enabled cameras to be effective sensing tools for tracking a target (i.e., estimating the position, orientation, and velocity state) in real time; however, the use of these sensors poses significant challenges. Specifically, a deficit of using image data for feedback is the lack of scale information for the target. This issue is commonly addressed by assuming known lengths between feature points attached to a target or by obtaining multiple views of the target, enabling geometric reconstruction of features (cf., [1–10]). Additionally, there is the potential for intermittent or permanent loss of image feedback due to the target leaving the limited field-of-view (FOV) of the camera, the target becoming occluded by surrounding objects in the scene, or the camera having poor sampling rates. These challenges are often addressed by using probabilistic or deterministic estimators that track the target when feedback is available, then use a predictor to propagate those estimates when feedback is not available.

Multiple views of a target may be achieved using a single camera over time (cf., [1–6, 9, 10]) or by a camera network providing simultaneous views of a target (cf., [7, 8]). The primary challenge that arises when using a single moving camera for tracking a moving target, generally referred to as the structure and motion from motion (SaMfM) problem (cf., [1–6, 9]), is that the velocity of the target is not measurable, requires the positive depth constraint, and continuous feedback of the target is required (cf., [1–4, 9, 10]). However, recent developments in [4–6] and [11] offer single camera approaches that alleviate these challenges. Alternatively, these challenges can be addressed by employing a camera network to generate simultaneous views of a target (cf., [7, 8]). However, these approaches often require specialized environments free of objects that may occlude the target, are intolerant to the target leaving the FOV of camera network, and require a high-density of cameras to ensure multiple views

of the target for the entire operating environment; increasing cost and computational requirements.

Our preliminary work in [12], developed an observer for estimating the Euclidean distances to features on a moving target using a network of stationary cameras, without requiring the traditional positive depth constraint. The result assumes the pose of the cameras in the network are known and that the target's features are initially contained in the shared FOV between two cameras, with sufficient parallax between the cameras to estimate scale. It also assumed that each camera's FOV is partially overlapping with the FOV of it's neighboring cameras. As the target travels through this environment, alternating single and multiple views of the target are available. Additionally, it is assumed that the intrinsic matrices for each camera are known, the motion of the target is not parallel to the direction to the object, and the position of the target is not at the origin of the camera. Using a Lyapunov-based stability analysis, the distance estimate errors were proven to converge exponentially, for both single and multi-view feedback regions. The approach did not assume *a priori* knowledge of the target's structure. Instead, structure is estimated when multiple views of the target are available. Also, through optical flow and estimates of the target's structure, the target's linear and angular velocities were measurable.

The intermittent feedback problem has traditionally been addressed using probabilistic estimators, e.g., Kalman filters (cf., [13–18]) and particle filters (cf., [19, 20]). These methods often linearize the feature's nonlinear dynamics, resulting in local convergence (cf., [13, 14, 16–18]), or are sample-based methods which only show optimal estimation in the limit as the number of samples approach infinity (cf., [19, 20]). Moreover, when proving the convergence of state estimates, probabilistic estimators typically require knowledge of the probability distribution of the uncertainties in the system,

resulting in convergence in mean. In contrast, deterministic estimators typically assume boundedness of uncertainties and disturbances in the analysis, yielding uniformly ultimately bounded results (cf., [6, 21]).

Using a single moving camera, [6] presents a deterministic approach for solving the intermittent feedback problem. When feedback for the target is available (i.e., the target is in the FOV), [6] uses pose (i.e., position and orientation) feedback data to approximate the motion model of the target. When feedback is not available (i.e., the target is not in the FOV), the approximated motion model is then used to predict the target's pose until feedback is regained. Using a Lyapunov-based switched systems approach, [6] demonstrates that the proposed estimator and predictor remains bounded, for all feedback and non-feedback cycles, provided that an average dwell-time condition is satisfied. This condition implies, over "k" cycles of losing and regaining feedback, the average time the target spends outside of a feedback region is sufficiently small such that the hybrid system remains bounded. For the tracking scenario presented in [6], the result is sufficient because the single camera can be commanded to track the target for an arbitrary length of time, prior to the target leaving the FOV of the camera. However, the average dwell-time analysis presented in [6] does not consider the problem where, if the target remains outside of a feedback region for too long, the target's positional uncertainty may grow greater than the camera's FOV, making it impractical for regaining feedback in many target tracking applications.

Our previous work in [21] addresses the aforementioned challenges by considering the scenario where a sparsely distributed network of stationary cameras, with non-overlapping FOVs, are tasked with tracking a target. Because the camera network is stationary, this problem formulation has no control over the length of time the target remains in a feedback region and demonstrates the need for regaining feedback prior to the uncertainty on the position of the target growing too large. Similar to [6], [21] develops an estimator and predictor which are proven to remain bounded, provided

the maximum and minimum dwell-time conditions for each feedback cycle are satisfied. However, these dwell-time conditions can only be satisfied if the neighboring cameras in the network are sufficiently close. Thus, [21] can only provide guidance on how to design stationary camera networks to certify a desired tracking performance requirement.

In Chapter 3, a deterministic estimator and predictor approach is developed for estimating the pose and velocity of a target. The system is characterized by two subsystems, when measurement feedback is available and unavailable. When a target is operating in the feedback region, the target's motion model is approximated online, using a neural network (NN) where a complementary concurrent learning (CCL) adaptation technique is used to estimate the ideal weights of the NN. The CCL adaptation technique is a weighted concurrent learning (CL) and integral concurrent learning (ICL) technique (cf. [4, 22–24]) that allows previously saved pose and velocity state data to improve the rate of convergence of the state estimates, where the persistence of excitation (PE) condition is replaced by a finite excitation (FE) condition, which is verified online. When measurement feedback is unavailable (i.e., the target leaves the FOV of the camera network), the motion model is used to propagate the target's state forward into the occluded region. Using a Lyapunov-based switched systems analysis, the estimator and predictor are proven to remain bounded provided the dwell-time conditions are satisfied. These dwell-time conditions dictate how long the target may remain outside the feedback regions, and how long the target must be observed when in the feedback regions. Moreover, an error growth analysis is developed using the dwell-time conditions, which relates the error dynamics to the physical network configuration.

In Chapter 4, the developments in Chapter 3 are generalized to incorporate velocity control of the camera network, where the cameras are constrained to non-overlapping operating regions where state feedback for the cameras are available. When the target enters an operating region and is observed by a camera belonging to the network (i.e., a

cooperative agent), a sliding mode controller (SMC) is used to regulate the cooperative agent's pose to track the target. Similar to Chapter 3, image feedback for the target is available when the target is contained in the cooperative agent's FOV. The target's motion model is approximated online when feedback is available using a NN where a CCL adaptation technique is used to estimate the ideal weights of the NN. When the target leaves an operating region, the cooperative agent in that region can no longer track the target, causing image feedback to become unavailable. When feedback is unavailable, the approximated motion model is used to propagate the target's state estimates through the occluded regions until the estimates intersect a neighboring operating region, informing the neighboring cooperative agent where to intercept the target to reestablish visual feedback. Using a Lyapunov-based switched systems approach, the proposed framework is proven to remain bounded provided the maximum and minimum dwell-time conditions for each feedback cycle are satisfied. These dwell-time conditions dictate how long feedback must be available and how long feedback may be unavailable, such that the system remains bounded and the target's positional uncertainty does not grow larger than the camera's FOV.

CHAPTER 2
SYSTEM MODELS

In this chapter, the system models used in Chapters 3 and 4 will be introduced.
Section 2.1 introduces the dynamic model for the target, where a sparsely distributed
network of stationary cameras is tasked with tracking a target. In Section 2.2, the dynamic
models for a network of mobile agents (i.e., cameras) and a target are introduced,
where the mobile network of cameras are tasked with tracking the target.

2.1   Dynamics for a Network of Stationary Cameras

Figure 2-1 illustrates the kinematic relationships between the moving object,
denoted by $\mathcal{M}$, and the cameras in the network. As shown in Figure 2-1, $\mathcal{F}_G$ represents
the inertial reference frame for the system with an arbitrary origin, denoted by o_g, and
basis $\left\{\underline{x}_G, \underline{y}_G, \underline{z}_G\right\}$, while $\mathcal{F}_m$ represent the object's body-fixed reference frame with
an origin located at m_1, representing an arbitrary feature point attached to the object,
with basis $\left\{\underline{x}_m, \underline{y}_m, \underline{z}_m\right\}$. For the camera network, $\left\{\mathcal{F}_{c_j}\right\}_{j=1}^C$ represents the set of
stationary camera reference frames, where $\mathcal{F}_{c_j}$ is the jth camera's reference frame and
$C \in \mathbb{Z}_{>1}$ is the number of cameras in the network. Also, each camera's reference frame
has an origin located at the principal point of the camera, denoted by c_j, with basis
$\left\{\underline{x}_{c_j}, \underline{y}_{c_j}, \underline{z}_{c_j}\right\}$, where $\underline{z}_{c_j} \in \mathbb{R}^3$ axis is along the viewing direction and co-linear with the
optical axis, $\underline{y}_{c_j} \in \mathbb{R}^3$ is parallel with and facing the image plane, and $\underline{x}_{c_j} \triangleq \underline{y}_{c_j} \times \underline{z}_{c_j} \in \mathbb{R}^3$.
Let $\underline{p}_{m_i/c_j}(t) \in \mathbb{R}^3$ represent the position of feature point m_i with respect to c_j, in $\mathcal{F}_{c_j}$. Let
$\underline{p}_{m_i/G}(t) \in \mathbb{R}^3$ represent the position of feature point m_i with respect to o_g, in $\mathcal{F}_G$. The
structure of $\mathcal{M}$ is denoted by $\underline{p}_{m_i/m_1} \in \mathbb{R}^3$, which represents the position of feature point
m_i with respect to m_1, in $\mathcal{F}_m$. The Euclidean space contained within the jth camera's
field-of-view (FOV) is denoted by $\mathcal{V}_{c_j} \subset \mathbb{R}^3$, where the set of these spaces are denoted
by $\mathcal{V}_C \triangleq \left\{\mathcal{V}_{c_j}\right\}_{j=1}^C$. Additionally, the indexing sequence for the cameras serve only to
identify the cameras in the network and may not be representative of the jth camera's
immediate neighbors (e.g., $\mathcal{V}_{c_2}$ may not be in close proximity to $\mathcal{V}_{c_1}$ or $\mathcal{V}_{c_3}$). For the target
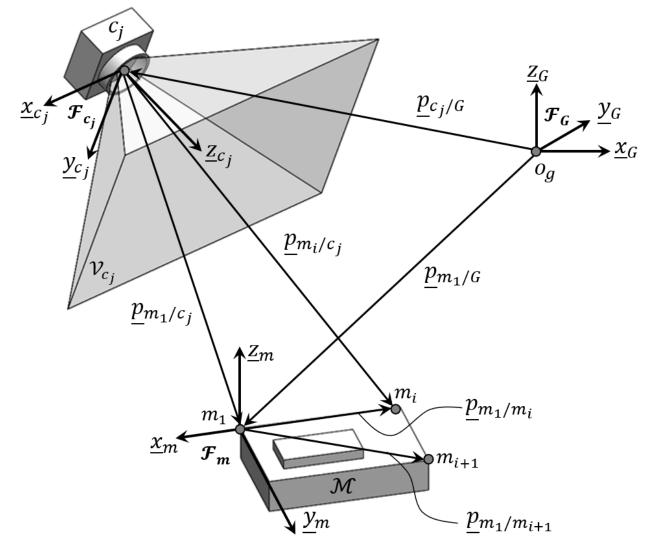
Figure 2-1. Single-view geometry of features on a moving object.

to be within the FOV of the jth camera, $\mathcal{P}_G \subset \mathcal{V}_{c_j}$, where $\mathcal{P}_G \triangleq \left\{ \underline{p}_{m_i/G} \right\}_{i=1}^m$ and $m \in \mathbb{Z}_{\geq 4}$ represents the number of features attached to the target.

The linear velocity of the moving object is determined by the kinematic relationship between the features on $\mathcal{M}$ and the inertial fixed reference frame and is denoted by $\underline{v}_{m_1/G}(t) \in \mathbb{R}^3$, where $\underline{v}_{m_1/G}(t) = \underline{\dot{p}}_{m_i/G}(t)$. The angular velocity of $\mathcal{M}$ with respect to the inertial fixed reference frame is described by (see [25, Chapter 3.4])

$$\dot{q} = \frac{1}{2} B\left(q\left(t\right)\right) \underline{\omega}_{m/G}\left(t\right), \tag{2–1}$$

where $\underline{\omega}_{m/G}(t) \triangleq \begin{bmatrix} \omega_x & \omega_y & \omega_z \end{bmatrix}^T \in \mathbb{R}^3$ is the angular velocity of $\mathcal{M}$ with respect to $\mathcal{F}_G$, q is the quaternion parameterization of $R_{m/G}(t)$ which is a rotation matrix representing the orientation between $\mathcal{F}_m$ and $\mathcal{F}_G$. Furthermore, $B\left(q\left(t\right)\right) : \mathcal{S}^4 \to \mathbb{R}^{4 \times 3}$ is defined as $B\left(q\left(t\right)\right) \triangleq \begin{bmatrix} -q_v^T\left(t\right) \\ q_0\left(t\right) I_3 + q_v^\times\left(t\right) \end{bmatrix}$ and has the pseudo-inverse property $B\left(q\left(t\right)\right)^T B\left(q\left(t\right)\right) = I_{3 \times 3}$, where $(\cdot)^\times : \mathbb{R}^3 \to \mathbb{R}^{3 \times 3}$ represents the skew operator, $q\left(t\right) \triangleq \begin{bmatrix} q_0\left(t\right) & q_v^T\left(t\right) \end{bmatrix}^T \in \mathcal{S}^4$ has the standard basis $\{1, \, i, \, j, \, k\}$, $\mathcal{S}^4 \triangleq \left\{ x \in \mathbb{R}^4 | x^T x = 1 \right\}$, and $q_0\left(t\right)$ and $q_v\left(t\right)$ represent the scalar and vector components of $q\left(t\right)$, respectively.

2.2 Dynamics for a Network of Mobile Cameras

Figure 2-2 illustrates the kinematic relationships between the jth cooperative agent, denoted by $\mathcal{C}_j$, and the target agent, denoted by $\mathcal{M}$. As shown in Figure 2-2, $\mathcal{F}_G$ represents the inertial reference frame which has an arbitrarily selected origin, denoted by o_g, and the basis $\left\{ \underline{x}_G, \underline{y}_G, \underline{z}_G \right\}$, while $\mathcal{F}_m$ represents the target agent's body-fixed reference frame with an origin located at m (i.e., an arbitrarily selected feature point attached to the rigid body), with the basis $\left\{ \underline{x}_m, \underline{y}_m, \underline{z}_m \right\}$. For the network of cooperative agents, $\left\{ \mathcal{F}_{c_j} \right\}_{j=1}^C$ represents the set of body-fixed reference frames belonging to the agents, where $\mathcal{F}_{c_j}$ is $\mathcal{C}_j$'s reference frame, and $C \in \mathbb{Z}_{>1}$ is the number of agents in the network. Also, each $\mathcal{F}_{c_j}$ has an origin located at the principal point of the agent's camera, denoted by c_j, with the basis $\left\{ \underline{x}_{c_j}, \underline{y}_{c_j}, \underline{z}_{c_j} \right\}$, where the $\underline{z}_{c_j} \in \mathbb{R}^3$ axis is along
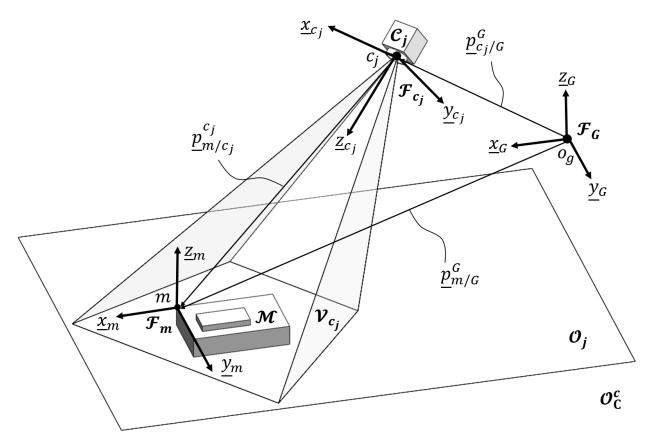
Figure 2-2. Kinematic relationship between cooperative agent and target agent.

the viewing direction and co-linear with the optical axis, $\underline{y}_{c_j} \in \mathbb{R}^3$ is along the image plane vertical, and $\underline{x}_{c_j} \in \mathbb{R}^3$ is along the image plane horizontal. The Euclidean space contained within $\mathcal{C}_j$'s FOV is denoted by $\mathcal{V}_{c_j} \subset \mathbb{R}^3$, where the set of these spaces are denoted by $\mathcal{V}_C \triangleq \{\mathcal{V}_{c_j}\}_{j=1}^{C}$. Each $\mathcal{C}_j$ is constrained to an operating region, denoted by $\mathcal{O}_j \subset \mathbb{R}^3$, where the set of these operating regions are denoted by $\mathcal{O}_C \triangleq \{\mathcal{O}_j\}_{j=1}^{C}$, and none of the operating regions overlap (i.e., $\mathcal{O}_j \cap \mathcal{O}_p = \emptyset$, where $p \in \{1, \ldots, C\} \setminus \{j\}$). Additionally, let $\mathcal{O}_C^c \triangleq \{x \in \mathcal{U} \mid x \notin \mathcal{O}_C\}$ describe the remaining space outside of $\mathcal{O}_C$, where $\mathcal{U} \in \mathbb{R}^3$ represents the entire tracking environment. Moreover, $\mathcal{O}_C$ represents the regions where image feedback for $\mathcal{M}$ is available, while $\mathcal{O}_C^c$ represents the region where feedback is unavailable.

2.2.1 Vehicle Dynamics

The kinematics used to represent $\mathcal{C}_j$'s linear velocity is described as

$$\dot{\underline{p}}_{c_j/G}^{G}(t) = u_{l,c_j}(t) + d_{l,c_j}(t), \tag{2--2}$$

where $\dot{\underline{p}}_{c_j/G}^{G}(t) \in \mathbb{R}^3$ represents the velocity of the $\mathcal{C}_j$'s origin (i.e., c_j) with respect to $\mathcal{F}_G$'s origin (i.e., o_g) expressed in $\mathcal{F}_G$, and $u_{l,c_j}(t) \in \mathbb{R}^3$ and $d_{l,c_j}(t) \in \mathbb{R}^3$ represents $\mathcal{C}_j$'s control input and exogenous disturbance along the basis $\{\underline{x}_{c_j}, \underline{y}_{c_j}, \underline{z}_{c_j}\}$, respectively. Additionally, the orientation dynamics of $\mathcal{C}_j$'s body-fixed reference frame (i.e., $\mathcal{F}_{c_j}$) with respect to $\mathcal{F}_G$ is described by

$$\dot{q}_{c_j/G}(t) = \frac{1}{2} B\left(q_{c_j/G}(t)\right) \left(u_{a,c_j}(t) + d_{a,c_j}(t)\right), \tag{2--3}$$

where $q_{c_j/G}(t) \in \mathbb{R}^4$ represents the quaternion parameterization of $R_{c_j/G}(t) \in \mathbb{R}^{3\times3}$, $R_{c_j/G}(t)$ is the rotation matrix representing the orientation of $\mathcal{F}_{c_j}$ with respect to $\mathcal{F}_G$, and $u_{a,c_j}(t) \in \mathbb{R}^3$ and $d_{a,c_j}(t) \in \mathbb{R}^3$ represents $\mathcal{C}_j$'s control input and exogenous disturbance about the basis $\{\underline{x}_{c_j}, \underline{y}_{c_j}, \underline{z}_{c_j}\}$, respectively.

2.2.2 Target Dynamics

As illustrated in Figure 2-2, the position of $\mathcal{M}$'s origin (i.e., m) with respect to o_g expressed in $\mathcal{F}_G$ is described by

$$\underline{p}^G_{m/G}(t) = \underline{p}^G_{c_j/G}(t) + R_{c_j/G}(t)\,\underline{p}^{c_j}_{m/c_j}(t)\,, \qquad (2\text{--}4)$$

where $\underline{p}^G_{c_j/G}(t) \in \mathbb{R}^3$ represents the position of c_j with respect to o_g expressed in $\mathcal{F}_G$ and $\underline{p}^{c_j}_{m/c_j}(t) \in \mathbb{R}^3$ is the position of m with respect to c_j expressed in $\mathcal{F}_{c_j}$. Taking the time-derivative of (2–4) yields

$$\underline{\dot{p}}^G_{m/c_j}(t) = \underline{\dot{p}}^G_{m/G}(t) - \underline{\dot{p}}^G_{c_j/G}(t) - \underline{\omega}^\times_{c_j/G}(t)\,\underline{p}^G_{m/c_j}(t)\,, \qquad (2\text{--}5)$$

where $\underline{\dot{p}}^G_{m/G}(t) \in \mathbb{R}^3$ is the linear velocity of m with respect to o_g expressed in $\mathcal{F}_G$, and $\underline{\omega}_{c_j/G}(t) \triangleq \begin{bmatrix} \omega_{x,c_j/G} & \omega_{y,c_j/G} & \omega_{z,c_j/G} \end{bmatrix}^T \in \mathbb{R}^3$ is the angular velocity of $\mathcal{F}_{c_j}$ with respect to $\mathcal{F}_G$. Additionally, the orientation dynamics of $\mathcal{M}$'s body-fixed reference frame (i.e., $\mathcal{F}_m$) with respect to $\mathcal{F}_{c_j}$ is described by

$$\begin{aligned} \dot{q}_{m/c_j}(t) = & \\ & \tfrac{1}{2} B\left(q_{m/c_j}(t)\right) R^T_{m/c_j}(t)\left(\underline{\omega}_{m/G}(t) - \underline{\omega}_{c_j/G}(t)\right), \end{aligned} \qquad (2\text{--}6)$$

where $q_{m/c_j}(t) \in \mathbb{R}^4$ is the quaternion parameterization of $R_{m/c_j}(t) \in \mathbb{R}^{3\times 3}$, $R_{m/c_j}(t)$ is the rotation matrix representing the orientation of $\mathcal{F}_m$ with respect to $\mathcal{F}_{c_j}$, and $\underline{\omega}_{m/G}(t) \triangleq \begin{bmatrix} \omega_{x,m/G} & \omega_{y,m/G} & \omega_{z,m/G} \end{bmatrix}^T \in \mathbb{R}^3$ is the angular velocity of $\mathcal{F}_m$ with respect to $\mathcal{F}_G$.

CHAPTER 3
TARGET TRACKING IN THE PRESENCE OF INTERMITTENT MEASUREMENTS BY
A SPARSELY DISTRIBUTED NETWORK OF STATIONARY CAMERAS

In this chapter, an estimator and predictor framework is developed for approximating
the pose and motion model of a moving target, using a sparsely distributed network
of stationary cameras. As the target navigates through the tracking environment, the
target is intermittently observed by the camera network, causing periods when visual
feedback is available and unavailable. While feedback is available, measurements of
the target's state are recorded and used to approximate the target's motion model. This
motion model is then used in a predictor, when feedback is not available, to propagate
the target's state estimate into the non-feedback regions. Using a Lyapunov-based
switched systems approach, the estimator and predictor are proven to remain bounded
provided minimum and maximum dwell-time conditions are satisfied. Additionally, an
error growth analysis is developed using these dwell-time conditions, which relates the
target's positional uncertainties to the physical network configuration.

3.1 Estimator and Predictor Design

The objective of this chapter is to develop a method for estimating a moving object's
pose, despite intermittent measurements that results from the object transitioning
between non-overlapping FOVs in a camera network. To do this, an estimator and
predictor framework are developed to estimate the object's pose and motion model
when feedback is available, and then uses the motion model to propagate the pose
estimates through the occluded regions until measurement feedback is regained. Figure
3-1 illustrates an example of the proposed framework, where $\mathcal{M}$ has traveled from the
$j - 1$th camera to the $j + 1$th camera. Measurement feedback is available when $\mathcal{M}$
travels through $\mathcal{V}_{c_{j-1}} \rightarrow \mathcal{V}_{c_{j+1}}$, where estimates of $\mathcal{M}$'s pose is represented by the solid
trajectory, and predictions of $\mathcal{M}$'s pose is represented by the dashed trajectory. Let $\eta\left(t\right)$
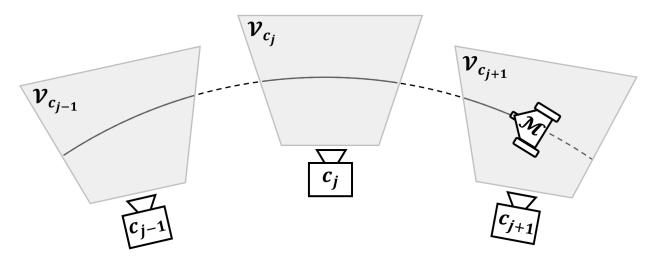
Figure 3-1. Example of the target traveling between FOVs in camera network.

be a state vector that stacks $\mathcal{M}$'s position and orientation, which is defined as

$$\eta\left(t\right) \triangleq \left[\begin{array}{cc} \underline{p}_{m_1/G}^{T}\left(t\right) & q^{T}\left(t\right) \end{array}\right]^{T}.$$

Assumption 3.1. The state $\eta\left(t\right)$ is bounded (i.e., $\eta\left(t\right) \in \chi$, where $\chi \subset \mathbb{R}^7$ is a convex, compact set).

Taking the time derivative of $\eta\left(t\right)$ and substituting (2–1) yields

$$\dot{\eta}\left(t\right) = \left[\begin{array}{c} \underline{v}_{m_1/G}\left(t\right) \\ \frac{1}{2}B\left(q\left(t\right)\right)\underline{\omega}_{m/G}\left(t\right) \end{array}\right], \tag{3–1}$$

which can be determined when image feedback is available.

Assumption 3.2. Measurement for $\eta\left(t\right)$ and $\dot{\eta}\left(t\right)$ are available when $\mathcal{M}$ is contained in the FOV of the camera network (i.e., when $\mathcal{P}_G \subset \mathcal{V}_C$).

Remark 3.1. By using an approach similar to [12], when the target is contained in the FOV of the camera network, estimates of the target's pose, linear velocity, and angular velocity can be obtained.

Assumption 3.3. The object's velocity state is described by a locally Lipschitz function of the object's pose, which is not explicitly time dependent (i.e., $\underline{v}_{m_1/G}\left(t\right) = \varphi_1\left(\eta\left(t\right)\right)$ and $\underline{\omega}_{m/G}\left(t\right) = \varphi_2\left(\eta\left(t\right)\right)$, where $\varphi_1, \varphi_2 : \mathbb{R}^7 \to \mathbb{R}^3$ are bounded).

Remark 3.2. Assumption 3.3 guarantees there exists a function that can be approximated, using universal function approximators (e.g., neural networks (NN)), that describes $\dot{\eta}(t)$ to an arbitrary level of accuracy via the Stone–Weierstrass Theorem [26] (i.e., $\bar{\varepsilon}$ can be made arbitrary small). Furthermore, the Stone–Weierstrass Theorem only ensures the approximation is accurate over a closed interval. Thus, dependence on $\eta(t)$ is allowed since it is bounded via Assumption 3.1. Specifically, from Assumption 3.3, $\dot{\eta}(t)$ can be approximated as

$$
\begin{aligned}
\dot{\eta}(t) &= \begin{bmatrix} \varphi_1(\eta(t)) \\ \frac{1}{2}B(q(t))\varphi_2(\eta(t)) \end{bmatrix} \\
&= W^T \sigma(\eta(t)) + \varepsilon(\eta(t)),
\end{aligned}
\tag{3--2}
$$

where $W \in \mathbb{R}^{p \times 7}$ is a matrix of unknown ideal weights, $\sigma : \mathbb{R}^7 \to \mathbb{R}^p$ is a known, bounded, and locally Lipschitz vector of basis functions, p represents the number of nodes in the NN, $\varepsilon : \mathbb{R}^7 \to \mathbb{R}^7$ is a function approximation residual that is locally Lipschitz and can be bounded *a priori* by $\bar{\varepsilon} \triangleq \sup_{\eta \in \chi, t \in [0,\infty)} \|\varepsilon(\eta(t))\|$, and $\|\cdot\|$ is the Euclidean norm operator.

Let the object's state estimation error, denoted by $\widetilde{\eta}(t) \in \mathbb{R}^7$, be defined as

$$
\widetilde{\eta}(t) \triangleq \eta(t) - \hat{\eta}(t),
\tag{3--3}
$$

where $\hat{\eta}(t) \in \mathbb{R}^7$ is the estimate of $\eta(t)$. Taking the time derivative of (3–3) and substituting (3–2) results in the closed-loop error system

$$
\dot{\widetilde{\eta}}(t) = W^T \sigma(\eta(t)) + \varepsilon(\eta(t)) - \dot{\hat{\eta}}(t),
\tag{3--4}
$$

where $\dot{\hat{\eta}}(t) \in \mathbb{R}^7$ is the pose estimator update law. Additionally, the NN weight estimation error, $\widetilde{W}(t) \in \mathbb{R}^{p \times 7}$, is defined as

$$
\widetilde{W}(t) \triangleq W - \hat{W}(t),
\tag{3--5}
$$

22

where $\hat{W}(t) \in \mathbb{R}^{p \times 7}$ is the estimate of the ideal weights. Taking the time derivative of (3–5) yields

$$\dot{\widetilde{W}}(t) = -\dot{\hat{W}}(t),\tag{3–6}$$

where $\dot{\hat{W}}(t) \in \mathbb{R}^{p \times 7}$ is the weight estimator update law. Stacking the state and weight estimation errors results in the error vector, $\xi(t) \in \mathbb{R}^{7+7p}$, which is defined as

$$\xi(t) \triangleq \left[\begin{array}{cc} \tilde{\eta}^T(t) & vec\left(\widetilde{W}(t)\right)^T \end{array}\right]^T,\tag{3–7}$$

where $vec(\cdot)$ denotes a stack of the columns of $(\cdot)$. Using the definition for $\xi(t)$, the estimation objective is to design $\dot{\hat{\eta}}(t)$ and $\dot{\hat{W}}(t)$ so that $\xi(t) \in \mathcal{L}_\infty$.

3.1.1 State and Motion Model Estimator - Update Design

Informed by the subsequent stability analysis, when feedback is available, the pose estimator update law is

$$\dot{\hat{\eta}}(t) = \hat{W}^T(t)\sigma(\eta(t)) + k_1\tilde{\eta}(t) + k_2\mathsf{sgn}(\tilde{\eta}(t)),\tag{3–8}$$

where $\mathsf{sgn}(\cdot)$ is the signum function, and $k_1, k_2 \in \mathbb{R}_{>0}$ are constant, positive control gains. Substituting (3–8) into (3–4) yields the closed-loop error system for the pose estimator as

$$\dot{\tilde{\eta}}(t) = \widetilde{W}^T(t)\sigma(\eta(t)) + \varepsilon(\eta(t)) - k_1\tilde{\eta}(t) - k_2\mathsf{sgn}(\tilde{\eta}(t)).\tag{3–9}$$

The weight update law for estimating the ideal weight of the motion model is designed as

$$\begin{aligned}\dot{\hat{W}}(t) =\mathsf{proj}\Big(&\Gamma\sigma(\eta(t))\tilde{\eta}^T(t)\\&+\alpha k_{CL}\Gamma\sum_{i=1}^{N}\mathcal{Y}_i^T\left(\Delta\eta_i^T - \mathcal{Y}_i\hat{W}(t)\right)\\&+(1-\alpha)k_{CL}\Gamma\sum_{k=1}^{N}Y_k^T\left(\dot{\eta}_k^T - Y_k\hat{W}(t)\right)\Big),\end{aligned}\tag{3–10}$$

23

where $k_{CL} \in \mathbb{R}_{>0}$ and $\alpha \in [0, 1]$ are constant control gains, $\Gamma \in \mathbb{R}^{p \times p}$ is a constant, positive definite and symmetric control gains, and $\mathrm{proj}\,(\cdot)$ is a smooth projection operator (see [27, Appendix E], [28, Remark 3.7]) with state and velocity bounds which are known under Assumptions 3.1 and 3.3. Additionally, $N \in \mathbb{Z}_{>p}$ represents the size of the history stacks, $\mathcal{Y}_i \triangleq \mathcal{Y}(t_i)$ and $\Delta \eta_i \triangleq \eta(t_i) - \eta(t_i - \Delta t)$ represent recorded data at $t_i \in [\Delta t, t]$, where $\mathcal{Y}(t) \triangleq \int_{t-\Delta t}^{t} \sigma^T(\eta(\tau))\, d\tau$, and $\Delta t \in \mathbb{R}_{>0}$ is an integration window. Also, $Y_k \triangleq Y(t_k)$ and $\dot{\eta}_k \triangleq \dot{\eta}(t_k)$ represent recorded data at $t_k \in [0, t]$, where $Y(t) \triangleq \sigma^T(\eta(t))$.[1] By using a weighted CL and ICL technique in the design of (3–10), recorded pose and velocity data can be used to influence the rate of convergence of the ideal weight estimates. Moreover, (3–2) over the time interval $[t - \Delta t,\, t]$ yields

$$\Delta \eta^T(t) = \mathcal{Y}(t)\, W + \mathcal{E}(t), \tag{3–11}$$

$\forall t \in [\Delta t, \infty)$, where $\mathcal{E}(t) \triangleq \int_{t-\Delta t}^{t} \varepsilon^T(\eta(\tau))\, d\tau$. Evaluating (3–11) at $t = t_i$ yields

$$\Delta \eta_i^T = \mathcal{Y}_i W + \mathcal{E}_i, \tag{3–12}$$

where $\mathcal{E}_i \triangleq \mathcal{E}(t_i)$. Also, evaluating (3–2) at $t = t_k$ yields

$$\dot{\eta}_k^T = Y_k W + \varepsilon_k^T, \tag{3–13}$$

where $\varepsilon_k \triangleq \varepsilon(\eta(t_k))$. Substituting (3–12) and (3–13) into (3–10), yields a simplified expression for the weight update law that can then be substituted into (3–6) to yield the closed-loop error system for the weight estimator as

---

[1] The indices for $\mathcal{Y}_i$ and Y_k are not necessarily the same (i.e., the recorded data in the history stacks may be updated asynchronously).

$$\dot{\widetilde{W}}(t) = -\text{proj}\left(\Gamma\sigma\left(\eta\left(t\right)\right)\tilde{\eta}\left(t\right)^{T} + k_{CL}\Gamma\Psi\left(t\right)\widetilde{W}\left(t\right)\right.$$
$$\left. + k_{CL}\Gamma\alpha\sum_{i=1}^{N}\mathcal{Y}_{i}^{T}\mathcal{E}_{i} + k_{CL}\Gamma\left(1-\alpha\right)\sum_{k=1}^{N}Y_{k}^{T}\varepsilon_{k}\right), \tag{3-14}$$

where $\Psi\left(t\right) \triangleq \alpha\sum_{i=1}^{N}\mathcal{Y}_{i}^{T}\mathcal{Y}_{i} + \left(1-\alpha\right)\sum_{k=1}^{N}Y_{k}^{T}Y_{k}$.

3.1.2 State and Motion Model Estimator - Predictor Design

When the moving object becomes occluded or travels outside the feedback region of the camera network, the pose estimates are propagated forward into the non-feedback region using the predictor update law,

$$\dot{\hat{\eta}}\left(t\right) = \text{proj}\left(\hat{W}^{T}\left(t\right)\sigma\left(\hat{\eta}\left(t\right)\right)\right). \tag{3-15}$$

Substituting (3–15) into (3–4) yields a closed-loop error system for the pose predictor as

$$\dot{\tilde{\eta}}\left(t\right) = \widetilde{W}^{T}\left(t\right)\sigma\left(\eta\left(t\right)\right) + \hat{W}^{T}\left(t\right)\widetilde{\sigma}\left(t\right) + \varepsilon\left(\eta\left(t\right)\right), \tag{3-16}$$

where $\widetilde{\sigma}\left(t\right) \triangleq \sigma\left(\eta\left(t\right)\right) - \sigma\left(\hat{\eta}\left(t\right)\right)$. Additionally, the ideal weight estimates are also updated when $\mathcal{M}$ is in the non-feedback regions using the recorded data (i.e., $\Psi\left(t\right)$), when measurements were available. The predictor's weight update law is designed as

$$\dot{\hat{W}}\left(t\right) = \text{proj}\left(k_{CL}\Gamma\alpha\sum_{i=1}^{N}\mathcal{Y}_{i}^{T}\left(\Delta\eta_{i} - \mathcal{Y}_{i}\hat{W}\left(t\right)\right) + k_{CL}\Gamma\left(1-\alpha\right)\sum_{k=1}^{N}Y_{k}^{T}\left(\dot{\eta}_{k}^{T} - Y_{k}\hat{W}\left(t\right)\right)\right). \tag{3-17}$$

Substituting (3–12) and (3–13) into (3–17), yields a simplified expression for the predictor's weight update law that is then substituted into (3–6) to yield a closed-loop error system for the ideal weight predictor as

$$\dot{\widetilde{W}}\left(t\right) = -\text{proj}\left(k_{CL}\Gamma\Psi\left(t\right)\widetilde{W}\left(t\right) + k_{CL}\Gamma\alpha\sum_{i=1}^{N}\mathcal{Y}_{i}^{T}\mathcal{E}_{i} + k_{CL}\Gamma\left(1-\alpha\right)\sum_{k=1}^{N}Y_{k}^{T}\varepsilon_{k}\right). \tag{3-18}$$

3.2 Analysis

As the target transitions between non-overlapping FOVs in the camera network, the system considered in this analysis is characterized by two modes. When the target is in the FOV of camera network (i.e., $\mathcal{P}_G \subset \mathcal{V}_C$), measurement feedback is available and the estimator in (3–8) and (3–10) is active. The time spent in the measurement feedback region is denoted by $\Delta t_n^{\mathsf{on}} \triangleq t_n^{\mathsf{off}} - t_n^{\mathsf{on}}$, where t_n^{on} and t_n^{off} represents the time when measurement feedback first became available and unavailable, respectively, and n represents the nth instance when the measurements became available. When the target leaves the FOV of camera network (i.e., $\mathcal{P}_G \not\subset \mathcal{V}_C$), measurement feedback is unavailable and the predictor in (3–15) and (3–17) is active. This period is denoted by $\Delta t_n^{\mathsf{off}} \triangleq t_{n+1}^{\mathsf{on}} - t_n^{\mathsf{off}}$, where t_{n+1}^{on} represents the next instance when feedback is available. Lemmas 3.1 considers the mode when measurement feedback in available, while Lemma 3.2 considers the mode when feedback is not available.

Due to the weighted CL and ICL technique in (3–10), the measurement update mode is partitioned into two sub-systems, each dependent on if the history stacks (i.e., $\Psi(t)$) meet the finite excitation condition in the following assumption.

Assumption 3.4. At time denoted by $T > 0$, there exists a positive constant $\underline{\lambda} \in \mathbb{R}$ such that

$$\forall t \geq T,\ \lambda_{\min}\left\{\Psi(t)\right\} \geq \underline{\lambda}, \tag{3–19}$$

where $\lambda_{\min}\left\{\cdot\right\}$ refers to the minimum eigenvalue of $\{\cdot\}$.

When the target first enters $\mathcal{V}_C$, the history stack contains insufficiently rich excitation data (i.e., Assumption 3.4 is not met). The lack of rich excitation data reduces the performance of the estimator, as shown in Lemma 3.1; however, the estimator remains bounded. As more measurements become available, techniques like the singular value maximization algorithm in [29] are used to add and remove data in the history stack to maximize the minimum eigenvalue of $\Psi(t)$. After a finite period of time, the history stack is populated with sufficiently rich data and Assumption 3.4 is met at time T. Lemma

26

3.1 shows that for all $t > T$, by using the history stack in the adaptive update law, the estimator converges exponentially to an arbitrarily small bound. Furthermore, the history stack collected during $t \in [t_n^{\text{on}}, t_n^{\text{off}})$ is also used in the predictor, when $t \in [t_n^{\text{off}}, t_{n+1}^{\text{on}})$.

The Lyapunov-based analysis in the subsequent development use the Lyapunov function candidate

$$V\left(\xi\left(t\right)\right) \triangleq \frac{1}{2}\widetilde{\eta}^T\left(t\right)\widetilde{\eta}\left(t\right) + \frac{1}{2}\text{tr}\left(\widetilde{W}^T\left(t\right)\Gamma^{-1}\widetilde{W}\left(t\right)\right), \tag{3–20}$$

where $V : \mathbb{R}^{7+7p} \to \mathbb{R}$. To facilitate the stability analysis, (3–20) can be bounded by $\frac{1}{2}\gamma_1\left\|\xi\left(t\right)\right\|^2 \leq V\left(\xi\left(t\right)\right) \leq \frac{1}{2}\gamma_2\left\|\xi\left(t\right)\right\|^2$, where $\gamma_1 \triangleq \min\left\{1, \lambda_{min}\left\{\Gamma^{-1}\right\}\right\}$, $\gamma_2 \triangleq \max\left\{1, \lambda_{max}\left\{\Gamma^{-1}\right\}\right\}$, $\lambda_{max}\left\{\cdot\right\}$ refers to the maximum eigenvalue of $\left\{\cdot\right\}$, and $\min\left\{\cdot\right\}$ and $\max\left\{\cdot\right\}$ returns the minimum and maximum value in the set $\left\{\cdot\right\}$, respectively. Additionally, because of the projection operator in (3–10) and (3–17), $\hat{W}\left(t\right) \leq \left\|\hat{W}\left(t\right)\right\| \leq \dot{\eta}_{max}$, where $\dot{\eta}_{max} \in \mathbb{R}$ denotes a known bounding constant that is obtained from some knowledge about $\mathcal{M}$'s maximum linear and angular velocities. Also, $\left\|W\right\| \leq \dot{\eta}_{max}$, resulting in $\widetilde{W}\left(t\right) \leq \left\|\widetilde{W}\left(t\right)\right\| \leq 2\dot{\eta}_{max}$. Using these bounds, $V\left(\xi\left(t\right)\right) \leq \frac{1}{2}\left\|\tilde{\eta}\left(t\right)\right\|^2 + c_2$, where $c_2 \triangleq 2\lambda_{max}\left\{\Gamma^{-1}\right\}\dot{\eta}_{max}^2 \in \mathbb{R}_{>0}$ is a positive constant. Furthermore, taking the time derivative of (3–20) yields an expression that incorporates the closed-loop error systems, $\dot{\tilde{\eta}}\left(t\right)$ and $\dot{\widetilde{W}}\left(t\right)$, which is described as

$$\dot{V}\left(\xi\left(t\right)\right) = \widetilde{\eta}^T\left(t\right)\dot{\tilde{\eta}}\left(t\right) + \text{tr}\left(\widetilde{W}^T\left(t\right)\Gamma^{-1}\dot{\widetilde{W}}\left(t\right)\right). \tag{3–21}$$

3.2.1 Estimator - Stability Analysis

Lemma 3.1. *The estimator in (3–8) and (3–10) remains bounded during* $t \in [t_n^{\text{on}}, t_n^{\text{off}})$.

Proof. Considering the period where $t \in [t_n^{\text{on}}, t_n^{\text{off}}) \cap [0, T)$ (i.e., Assumption 3.4 is not met), substituting (3–9) and (3–14) into (3–21) and simplifying yields

$$\dot{V}\left(\xi\left(t\right)\right) \leq -k_1\left\|\tilde{\eta}\left(t\right)\right\|^2 + c_1, \tag{3–22}$$

where $c_1 \triangleq 2k_{CL}N\dot{\eta}_{max}\bar{\varepsilon}(\alpha\Delta t + 1 - \alpha)$ is a positive constant, and $k_2 > \bar{\varepsilon}$. Using the bounds on (3–20), (3–22) can be bounded by

$$\dot{V}(\xi(t)) \leq -2k_1 V(\xi(t)) + 2k_1 c_2 + c_1. \tag{3–23}$$

Using the Comparison Lemma [30, Lemma 3.4],

$$V(\xi(t)) \leq V(\xi(t_n^{\mathsf{on}})) \exp\left[-\lambda_D(t - t_n^{\mathsf{on}})\right] + \beta_1, \tag{3–24}$$

$\forall t \in [t_n^{\mathsf{on}}, t_n^{\mathsf{off}}) \cap [0, T)$, where $\beta_1 \triangleq \frac{c_1}{2k_1} + c_2$ and $\lambda_D \triangleq 2k_1$ are positive constants.

After sufficient data is collected and $t \in [t_n^{\mathsf{on}}, t_n^{\mathsf{off}}) \cap [T, \infty)$ (i.e., Assumption 3.4 is met), substituting (3–9) and (3–14) into (3–21) and simplifying yields

$$\dot{V}(\xi(t)) \leq -\min\{k_1, \lambda_{CL}\} \|\xi(t)\|^2 + c_1, \tag{3–25}$$

where $\lambda_{CL} \triangleq k_{CL}\lambda_{min}\{\Psi(t)\}$ and $k_2 > \bar{\varepsilon}$. Using the bounds on (3–20), (3–25) can be bounded by

$$\dot{V}(\xi(t)) \leq -\lambda_{D,T} V(\xi(t)) + c_1, \tag{3–26}$$

where $\lambda_{D,T} \triangleq \frac{2\min\{k_1, \lambda_{CL}\}}{\max\{1, \lambda_{max}\{\Gamma^{-1}\}\}}$.

Using the Comparison Lemma [30, Lemma 3.4],

$$V(\xi(t)) \leq V(\xi(t_n^{\mathsf{on}})) \exp\left[-\lambda_{D,T}(t - t_n^{on})\right] + c_{UB}, \tag{3–27}$$

$\forall t \in [t_n^{\mathsf{on}}, t_n^{\mathsf{off}}) \cap [T, \infty)$, where $c_{UB} \triangleq \frac{c_1 \max\{1, \lambda_{max}\{\Gamma^{-1}\}\}}{2\min\{k_1, \lambda_{CL}\}}$. $\qquad\square$

3.2.2 Predictor - Stability Analysis

Lemma 3.2. *The predictor in (3–15) and (3–17) remains bounded during* $t \in [t_n^{\mathsf{off}}, t_{n+1}^{\mathsf{on}})$.

Proof. Substituting (3–16) and (3–18) into (3–21) and simplifying yields

$$\dot{V}\left(\xi\left(t\right)\right) \le \frac{1}{2}\left\|\xi\left(t\right)\right\|^2 + c_3, \tag{3–28}$$

where $c_3 \triangleq \frac{1}{2}\left(4\dot{\eta}_{max} + \bar{\varepsilon}\right)^2 + c_1$. Using the bounds on (3–20), (3–28) can be bounded by

$$\dot{V}\left(\xi\left(t\right)\right) \le \frac{1}{\min\left\{1, \lambda_{min}\left\{\Gamma^{-1}\right\}\right\}} V(\xi\left(t\right)) + c_3. \tag{3–29}$$

Using the Comparison Lemma [30, Lemma 3.4],

$$V\left(\xi\left(t\right)\right) \le V\left(\xi\left(t_n^{\mathsf{off}}\right)\right) \exp\left[\lambda_G\left(t - t_n^{\mathsf{off}}\right)\right], \tag{3–30}$$

$\forall t \in [t_n^{\mathsf{off}}, t_{n+1}^{\mathsf{on}})$, where $\lambda_G \triangleq \frac{1}{\min\{1, \lambda_{min}\{\Gamma^{-1}\}\}}$. $\qquad\square$

3.2.3 Dwell-Time Analysis

In the following dwell-time analysis, a cycle refers to periods when measurement feedback is available (i.e, $t \in [t_n^{\mathsf{on}}, t_n^{\mathsf{off}})$), and unavailable (i.e., $t \in [t_n^{\mathsf{off}}, t_{n+1}^{\mathsf{on}})$).

Lemma 3.3. *The estimator in (3–8) and (3–10), and the predictor in (3–15) and (3–17) will remain bounded provided*

$$\Delta t_n^{off} \le \frac{1}{\lambda_G} \ln\left(\overline{V}/\underline{V}\right), \tag{3–31}$$

where $\overline{V}$ represents the maximum allowable value that $V\left(\xi\left(t\right)\right)$ may reach, during the period $t \in [t_n^{\mathsf{off}}, t_{n+1}^{\mathsf{on}})$, before the tracking objective becomes impractical (e.g., the uncertainty on $\eta\left(t\right)$ grows larger than the FOV of the neighboring cameras), and $\underline{V}$ represents the threshold that $V\left(\xi\left(t\right)\right)$ must decay below during the period $t \in [t_n^{\mathsf{on}}, t_n^{\mathsf{off}})$.

Proof. Consider a cycle to be a sequence of two sub-systems, starting with the sub-system defined in (3–24) for $t \in [t_n^{\mathsf{on}}, t_n^{\mathsf{off}})$ where feedback is available and the finite excitation condition is not met, and ending with (3–30) for $t \in [t_n^{\mathsf{off}}, t_{n+1}^{\mathsf{on}})$ where feedback is not available. Evaluating (3–24) at t_n^{off} yields

$$V\left(\xi\left(t_n^{\mathsf{off}}\right)\right) \le V\left(\xi\left(t_n^{\mathsf{on}}\right)\right) \exp\left[-\lambda_D(t_n^{\mathsf{off}} - t_n^{\mathsf{on}})\right] + \beta_1 \le \underline{V}. \tag{3–32}$$

29

Also, evaluating (3–30) at t_{n+1}^{on} yields

$$V\left(\xi\left(t_{n+1}^{\text{on}}\right)\right) \leq V\left(\xi\left(t_n^{\text{off}}\right)\right) \exp\left[\lambda_G\left(t_{n+1}^{\text{on}} - t_n^{\text{off}}\right)\right] \leq \overline{V}. \tag{3–33}$$

Combining (3–32) and (3–33) yields

$$\underline{V}\exp\left[\lambda_G\Delta t_n^{\text{off}}\right] \leq \overline{V}. \tag{3–34}$$

Solving for Δt_n^{off} yields the expression in (3–31). $\square$

Remark 3.3. The design of $\underline{V}$ can be considered an engineering parameter, that is dependent on the current network configuration and assumptions made about the target (e.g., $\dot{\eta}_{max}$).

Lemma 3.4. *After the dwell-time condition for Δt_n^{off} is satisfied and $\mathcal{M}$ enters the feedback region of the neighboring camera (i.e., the beginning of cycle $n + 1$), the estimator in (3–8) and (3–10) will converge to or below a user defined bound, $\underline{V}$, provided*

$$\Delta t_{n+1}^{on} \geq -\frac{1}{\lambda_D}\ln\left[\frac{\underline{V} - \beta_1}{\overline{V}}\right], \tag{3–35}$$

where $\underline{V} > \beta_1$.

Proof. The objective of this analysis is for

$$V\left(\xi\left(t_{n+1}^{\text{off}}\right)\right) \leq \underline{V}. \tag{3–36}$$

Considering the worst case scenario where the finite excitation condition is not met during the period where $t \in [t_{n+1}^{\text{on}}, t_{n+1}^{\text{off}})$, (3–24) is evaluated at t_{n+1}^{off}, yielding

$$V\left(\xi\left(t_{n+1}^{\text{off}}\right)\right) \leq V\left(\xi\left(t_{n+1}^{\text{on}}\right)\right) \exp\left[-\lambda_D(t_n^{\text{off}} - t_n^{\text{on}})\right] + \beta_1 \leq \underline{V}. \tag{3–37}$$

The right-hand side inequality of (3–37) can be simplified to

$$\overline{V}\exp\left[-\lambda_D\Delta t_n^{\text{on}}\right] + \beta_1 \leq \underline{V}. \tag{3–38}$$

Solving for Δt_n^{on} yields the expression in (3–35). □

Remark 3.4. Lemma 3.4 indicates the minimum time the target needs to remain in the feedback region of the following cycle for the estimator to remain stable, avoiding the scenario where the target only briefly crosses the outer boundaries of the feedback region. Furthermore, after sufficient excitation data is collected (i.e., $\Psi(t)$ meets the finite excitation condition in Assumption 3.4), the dwell-time condition can be replaced by

$$\Delta t_n^{\text{on}} \geq -\frac{1}{\lambda_{D,T}}\ln\left[\frac{\underline{V} - c_{UB}}{\overline{V}}\right],$$

resulting in a smaller Δt_n^{on} since $\lambda_{D,T} > \lambda_D$, or allowing $\underline{V}$ to be reduced, provided $\underline{V} > c_{UB}$.

Theorem 3.1. *Let* $\sigma_{n+1} \triangleq \{s_{n+1}, u_{n+1}\}$ *be a switching signal indicating whether the physical region of uncertainty on* $\underline{p}_{m_1/G}(t)$*, denoted by* $U_{max,n}(\varphi, \theta, t) \subset \mathbb{R}^3$*, will be contained within the FOV of another camera in the network,*

$$\sigma_{n+1} = \begin{cases} s_{n+1}, & \exists t : U_{max,n}(\varphi, \theta, t) \subset \mathcal{V}_C, \forall \varphi, \theta \\ u_{n+1}, & otherwise \end{cases},$$

where $t \in [t_n^{\text{off}}, t_n^{\text{off}} + \Delta t_n^{\text{off}})$*, and* $\varphi, \theta \in [0, 2\pi]$*. The estimator in (3–8) and (3–10), and predictor in (3–15) and (3–17) will remain bounded for the current network configuration provided*

$$\sigma_{n+1} = s_{n+1}, \forall n. \tag{3–39}$$

Proof. Using the predictor in (3–15) and (3–17), the uncertainty on $\underline{p}_{m_1/G}(t)$ can be represented by a sphere. Let
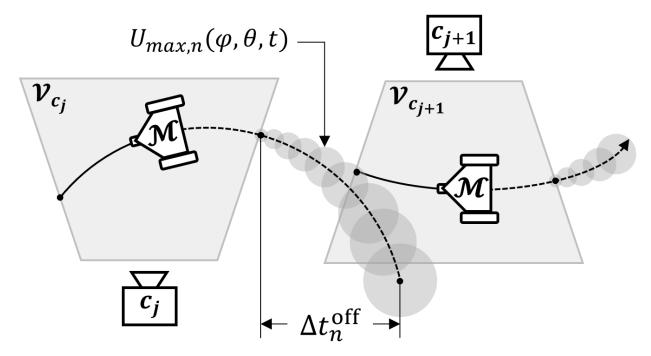
Figure 3-2. Evolution of $U_{max,n}(\varphi, \theta, t)$ during unstable sub-system.

$$\alpha_{max,n}(t) \triangleq 2v_{max}\left(t - t_n^{\mathsf{off}}\right), \tag{3–40}$$

represent the radius of the uncertainty sphere where $t \in [t_n^{\mathsf{off}}, t_n^{\mathsf{off}} + \Delta t_n^{\mathsf{off}})$. Assuming that $\mathcal{P}_G \subset \mathcal{V}_C$, the uncertainty sphere must be contained within $\mathcal{V}_C$, to guarantee that the dwell-time condition in Lemma 3.3 is satisfied. To guarantee that $\mathcal{M}$ remains within $\mathcal{V}_C$ for a sufficient amount of time such that $V\left(\xi\left(t_{n+1}^{\mathsf{off}}\right)\right) \leq \underline{V}$ (i.e., Lemma 3.4), let

$$\beta_{min,n+1} \triangleq v_{max}\Delta t_{n+1}^{\mathsf{on}} + \max\left\{\left\|\underline{p}_{m_i/G}(t) - \underline{p}_{m_1/G}(t)\right\| : \underline{p}_{m_i/G}(t) \in \mathcal{P}_G\right\}, \tag{3–41}$$

represent the maximum distance that $\mathcal{M}$ could travel within a single FOV in $\mathcal{V}_C$, such that Lemma 3.4 is satisfied. Let

$$U_{max,n}(\varphi, \theta, t) \triangleq \left\{\hat{\underline{p}}_{m_1/G}(t) + r_{max,n}(t)\begin{bmatrix} \mathsf{sin}\varphi\mathsf{cos}\theta \\ \mathsf{sin}\varphi\mathsf{sin}\theta \\ \mathsf{cos}\varphi \end{bmatrix}, \forall\varphi, \theta, \right\}, \tag{3–42}$$

represent the set of points on the surface of a sphere, centered at $\hat{\underline{p}}_{m_1/G}(t)$, with radius $r_{max,n}(t) \triangleq \alpha_{max,n}(t) + \beta_{min,n+1}$. If $U_{max,n}(\varphi, \theta, t)$ is contained within $\mathcal{V}_C$, during the period when $t \in [t_n^{\text{off}}, t_n^{\text{off}} + \Delta t_n^{\text{off}})$, then Lemma 3.3 will be satisfied for cycle n, and Lemma 3.4 will be satisfied for cycle $n + 1$. Thus, if this condition is held for all n cycles, then the dwell-time conditions for Δt_n^{off} and $\Delta t_{n+1}^{\text{on}}$ will be satisfied for the current network configuration, ensuring that the estimator and predictor will remain bounded throughout the target tracking objective. $\qquad\square$

Remark 3.5. Theorem 3.1 cannot be proven unless the target has been observed by the entire camera network (i.e., (3–39) holds). However, Lemmas 3.3 and 3.4 show that once measurement feedback is available for cycle n, σ_{n+1} can be determined and stability guarantees for the estimator and predictor could be made for the current and upcoming cycle. Moreover, this development provides a means of identifying areas of the camera network that lie ahead of the target, that may cause instabilities in the pose estimates. Furthermore, during the measurement feedback region of cycle n, if $\sigma_{n+1} = u_{n+1}$ (i.e., Lemma 3.3 will not be satisfied due to the network configuration), this development provides a time horizon within which the pose estimates can be trusted.

CHAPTER 4
TARGET TRACKING IN THE PRESENCE OF INTERMITTENT MEASUREMENTS BY A NETWORK OF MOBILE CAMERAS

In this chapter, a controller, estimator, and predictor framework is developed for tracking a moving target using a network of mobile cameras, with non-overlapping fields-of-views and operating regions. As the target navigates through the tracking environment, the target enters finite operating regions where a cooperative agent belonging to that region is tasked with tracking the target, establishing visual feedback. While feedback is available, measurements of the target's state are recorded and used to approximate the target's motion model. When the target exits the operating region, visual feedback becomes unavailable, and the approximated motion model is used in a predictor to propagate the target's state estimates through the non-feedback regions. Using a Lyapunov-based switched systems approach, the proposed framework is proven to be robust to intermittent feedback, and estimates of the target's pose and motion model are proven to remain bounded, provided that minimum and maximum dwell-time conditions are satisfied.

4.1 Control Design

The proposed target tracking framework requires the development of a controller, allowing the jth cooperative agent to track the target agent while the target is in the jth operating region (i.e., $\mathcal{M} \subset \mathcal{O}_j$). To facilitate the development of $\mathcal{C}_j$'s controller, let $\eta_{c_j/G}(t) \in \mathbb{R}^7$ be a state vector that stacks $\mathcal{C}_j$'s position and orientation, yielding

$$\eta_{c_j/G}(t) \triangleq \left[\begin{array}{cc} \left(\underline{p}_{c_j/G}^G(t)\right)^T & q_{c_j/G}^T(t) \end{array} \right]^T. \tag{4–1}$$

Taking the time-derivative of (4–1) and substituting in (2–2) and (2–3), yields $\mathcal{C}_j$'s velocity state vector,

$$\dot{\eta}_{c_j/G}(t) = \left[\begin{array}{c} u_{l,c_j}(t) + d_{l,c_j}(t) \\ \frac{1}{2}B\left(q_{c_j/G}(t)\right)\left(u_{a,c_j}(t) + d_{a,c_j}(t)\right) \end{array} \right]. \tag{4–2}$$

Let $\mathcal{C}_j$'s pose error system, denoted by $\widetilde{\eta}_{c_j/G}(t) \in \mathbb{R}^7$, be defined as

$$\widetilde{\eta}_{c_j/G}(t) \triangleq \eta_{c_j/G}(t) - \eta_{c_j/G,d}(t), \tag{4–3}$$

where $\eta_{c_j/G,d}(t) \triangleq \left[\left(\underline{p}_{c_j/G,d}^G(t) \right)^T \quad q_{c_j/G,d}^T(t) \right]^T \in \mathbb{R}^7$, $\underline{p}_{c_j/G,d}^G(t) \in \mathbb{R}^3$ represents the desired position of c_j with respect to o_g expressed in $\mathcal{F}_G$, and $q_{c_j/G,d}(t) \in \mathbb{R}^4$ represents the desired orientation of $\mathcal{F}_{c_j}$ with respect to $\mathcal{F}_G$.

Assumption 4.1. There exists a desired trajectory (i.e., $\eta_{c_j/G,d}(t)$), that is at least C^1 continuous, which allows $\mathcal{C}_j$ to track $\mathcal{M}$ (i.e., $\mathcal{M} \subset \mathcal{V}_{c_j}$) while $\mathcal{M} \subset \mathcal{O}_j$, and allows $\mathcal{C}_j$ to loiter arbitrarily within $\mathcal{O}_j$ while $\mathcal{M} \notin \mathcal{O}_j$.

Taking the time-derivative of (4–3) yields

$$\dot{\widetilde{\eta}}_{c_j/G}(t) = \dot{\eta}_{c_j/G}(t) - \dot{\eta}_{c_j/G,d}(t), \tag{4–4}$$

where $\dot{\eta}_{c_j/G,d}(t) \triangleq \left[\left(\underline{\dot{p}}_{c_j/G,d}^G(t) \right)^T \quad \dot{q}_{c_j/G,d}^T(t) \right]^T \in \mathbb{R}^7$, $\underline{\dot{p}}_{c_j/G,d}^G(t) \in \mathbb{R}^3$ represents the desired velocity of c_j with respect to o_g expressed in $\mathcal{F}_G$, and $\dot{q}_{c_j/G,d}(t) \in \mathbb{R}^4$ represents the desired angular velocity of $\mathcal{F}_{c_j}$ with respect to $\mathcal{F}_G$.

Assumption 4.2. Measurements for $\eta_{c_j/G}(t)$ and $\dot{\eta}_{c_j/G}(t)$ are available when $\mathcal{C}_j$ is operating within $\mathcal{O}_j$ (i.e., $\mathcal{C}_j \subset \mathcal{O}_j$).

Substituting (4–2) into (4–4) and simplifying yields

$$\dot{\widetilde{\eta}}_{c_j/G}(t) = u_{c_j}(t) + d_{c_j}(t) - \dot{\eta}_{c_j/G,d}(t), \tag{4–5}$$

where $u_{c_j}(t) \triangleq \left[u_{l,c_j}^T(t) \quad \left(\frac{1}{2} B\left(q_{c_j/G}(t) \right) u_{a,c_j}(t) \right)^T \right]^T \in \mathbb{R}^7$ and $d_{c_j}(t) \triangleq \left[d_{l,c_j}^T(t) \quad \left(\frac{1}{2} B\left(q_{c_j/G}(t) \right) d_{a,c_j}(t) \right)^T \right]^T \in \mathbb{R}^7$.

Assumption 4.3. The Euclidean norm of the exogenous disturbance $d_{c_j}(t)$ is bounded by $\left\| d_{c_j}(t) \right\| \le \overline{d}_{c_j} \in \mathbb{R}_{\ge 0}$.
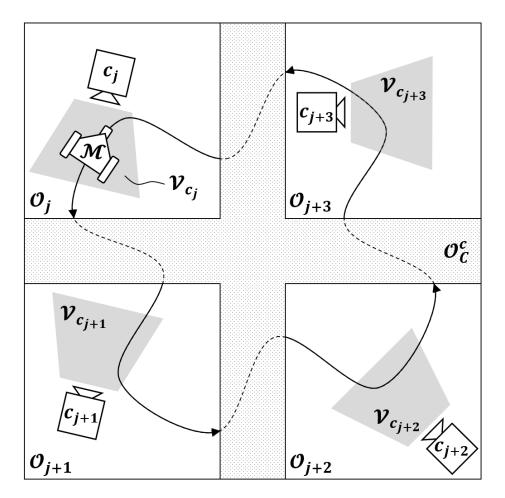
Figure 4-1. Generalized schematic of the target tracking objective.

The control objective is to design $\mathcal{C}_j$'s control input (i.e., $u_{c_j}(t)$) such that $\zeta_j(t) \in \mathcal{L}_\infty$, where $\zeta_j(t) \triangleq \widetilde{\eta}_{c_j/G}(t) \in \mathbb{R}^7$. Based on the subsequent stability analysis, $u_{c_j}(t)$ is designed as

$$u_{c_j}(t) \triangleq \dot{\eta}_{c_j/G,d}(t) - k_1 \widetilde{\eta}_{c_j/G}(t) - \overline{d}_{c_j} \mathsf{sgn}\left(\widetilde{\eta}_{c_j/G}(t)\right), \tag{4–6}$$

where $k_1 \in \mathbb{R}_{>0}$ is a constant control gain, and $\mathsf{sgn}(\cdot)$ is the signum function. Substituting (4–6) into (4–5) yields the closed-loop error system,

$$\dot{\widetilde{\eta}}_{c_j/G}(t) = -k_1 \widetilde{\eta}_{c_j/G}(t) + d_{c_j}(t) - \overline{d}_{c_j} \mathsf{sgn}\left(\widetilde{\eta}_{c_j/G}(t)\right). \tag{4–7}$$

4.2 Estimator and Predictor Design

To achieve the control objective, a method for estimating the pose of the target agent must be developed, that is robust to intermittent feedback. Figure 4-1 illustrates the target tracking objective where $\mathcal{M}$ is being tracked by $\mathcal{C}_j$, and $\mathcal{M}$ is approaching the outer boundary of $\mathcal{O}_j$. When $\mathcal{M}$ leaves $\mathcal{O}_j$ and enters the region where state feedback for $\mathcal{C}_j$ is no longer available (i.e., $\mathcal{M} \subset \mathcal{O}_C^c$), $\mathcal{C}_j$ will no longer be able to track $\mathcal{M}$, resulting in a loss of visual feedback for $\mathcal{M}$. Once $\mathcal{M}$ enters $\mathcal{O}_{j+1}$, $\mathcal{C}_{j+1}$ is tasked with tracking $\mathcal{M}$, reestablishing visual feedback of $\mathcal{M}$. The order of operating regions in Figure 4-1 is arbitrary. To accomplish the tracking objective, an estimator and predictor are developed to estimate $\mathcal{M}$'s pose and motion model when feedback is available (i.e., $\mathcal{M} \subset \mathcal{V}_{c_j}$), then the motion model is used to propagate the pose estimates through $\mathcal{O}_C^c$ when feedback is unavailable (i.e., $\mathcal{M} \notin \mathcal{V}_{c_j}$), informing $\mathcal{C}_{j+1}$ where to meet $\mathcal{M}$ in $\mathcal{O}_{j+1}$ to reestablish visual feedback. Let $\sigma_j^f(t) \in \{a, u\}$ be a switching signal indicating if feedback for $\mathcal{M}$ is available (i.e., $\sigma_j^f(t) = a$) or unavailable (i.e., $\sigma_j^f(t) = u$) while $\mathcal{M} \subset \mathcal{O}_j$.

To facilitate the design of the state estimator, let $\eta_{m/c_j}(t) \in \mathbb{R}^7$ be the pose state vector that stacks $\mathcal{M}$'s position and orientation, which is defined as

$$\eta_{m/c_j}(t) \triangleq \left[\ \left(\underline{p}_{m/c_j}^G(t) \right)^T \quad q_{m/c_j}^T(t) \ \right]^T. \tag{4–8}$$

Assumption 4.4. The state $\eta_{m/c_j}(t)$ is bounded (i.e., $\eta_{m/c_j}(t) \in \chi$, where $\chi \subset \mathbb{R}^7$ is a convex, compact set).

Taking the time-derivative of (4–8) and substituting in (2–5) and (2–1), yields the velocity state vector for $\mathcal{M}$, described by

$$\dot{\eta}_{m/c_j}(t) = \dot{\eta}_{m/G}(t) + f_j(\eta, t) \tag{4–9}$$

where $\dot{\eta}_{m/G}(t) \in \mathbb{R}^7$ represents $\mathcal{M}$'s velocity state vector with respect to $\mathcal{F}_G$ and is defined as

$$\dot{\eta}_{m/G}(t) \triangleq \begin{bmatrix} \dot{\underline{p}}^G_{m/G}(t) \\ \frac{1}{2} B\left(q_{m/c_j}(t)\right) R^T_{m/c_j}(t) \underline{\omega}_{m/G}(t) \end{bmatrix}, \tag{4–10}$$

and $f_j(\eta, t) \triangleq - \begin{bmatrix} \dot{\underline{p}}^G_{c_j/G}(t) + \underline{\omega}^\times_{c_j/G}(t) \underline{p}^G_{m/c_j}(t) \\ \frac{1}{2} B\left(q_{m/c_j}(t)\right) R^T_{m/c_j}(t) \underline{\omega}_{c_j/G}(t) \end{bmatrix} \in \mathbb{R}^7.$

Assumption 4.5. Measurements for $\eta_{m/c_j}(t)$ and $\dot{\eta}_{m/c_j}(t)$ are available when $\mathcal{M}$ is contained in the FOV of $\mathcal{C}_j$ (i.e., when $\mathcal{M} \subset \mathcal{V}_{c_j}$).

Remark 4.1. By using an approach similar to [12], when $\mathcal{M}$ is contained in the FOV of a camera in the network, estimates of the target's pose, linear velocity, and angular velocity can be obtained.

Assumption 4.6. The target's velocity state is described by a locally Lipschitz function of the target's pose, which is not explicitly time dependent (i.e., $\dot{\underline{p}}^G_{m/G}(t) = \varphi_1\left(\eta_{m/G}(t)\right)$ and $\underline{\omega}_{m/G}(t) = \varphi_2\left(\eta_{m/G}(t)\right)$, where $\varphi_1, \varphi_2 : \mathbb{R}^7 \to \mathbb{R}^3$ are bounded).

Remark 4.2. Assumption 4.6 guarantees there exists a function that can be approximated, using universal function approximators (e.g., neural networks (NN)), that describes $\dot{\eta}_{m/G}(t)$ to an arbitrary level of accuracy via the Stone–Weierstrass Theorem [26]. Furthermore, the Stone–Weierstrass Theorem only ensures the approximation is accurate over a closed interval. Thus, dependence on $\eta_{m/G}(t)$ is allowed since it is bounded via Assumption 4.4. Specifically, from Assumption 4.6, $\dot{\eta}_{m/G}(t)$ can be approximated as

$$\dot{\eta}_{m/G}(t) = \begin{bmatrix} \varphi_1\left(\eta_{m/G}(t)\right) \\ \frac{1}{2} B\left(q_{m/c_j}(t)\right) R^T_{m/c_j}(t) \varphi_2\left(\eta_{m/G}(t)\right) \end{bmatrix},$$
$$= W^T_j \sigma_j\left(\eta_{m/c_j}(t), \eta_{c_j/G}(t)\right) + \varepsilon_j\left(\eta_{m/c_j}(t), \eta_{c_j/G}(t)\right),$$

where $W_j \in \mathbb{R}^{p \times 7}$ is a matrix of unknown ideal weights, $\sigma_j : \mathbb{R}^7 \times \mathbb{R}^7 \to \mathbb{R}^p$ is a known, bounded, and locally Lipschitz vector of basis functions, $\varepsilon_j : \mathbb{R}^7 \times \mathbb{R}^7 \to \mathbb{R}^7$ is a function approximation residual that is locally Lipschitz and can be bounded *a*

priori by $\bar{\varepsilon} \triangleq \sup_{\eta_{m/c_j}(t), \eta_{c_j/G}(t) \in \chi, t \in [0,\infty)} \left\| \varepsilon_j \left(\eta_{m/c_j}(t), \eta_{c_j/G}(t) \right) \right\|$, $p \in \mathbb{Z}_{>0}$ represents the number of nodes in the NN, and $\|\cdot\|$ is the Euclidean norm operator. Furthermore, the "j" subscript for W_j, σ_j, and ε_j indicates that these terms belong only to $\mathcal{O}_j$ (i.e., each operating region is independently approximating $\mathcal{M}$'s motion model when $\mathcal{M} \subset \mathcal{O}_j$). The approximated motion model is then used in the predictor to propagate $\mathcal{M}$'s pose estimates through $\mathcal{O}_C^c$, until the pose estimates intersect a neighboring operating region, as illustrated in Figure 4-1. When $\mathcal{M}$ leaves $\mathcal{O}_j$, the previous motion model (i.e., $\Psi_j \left(t_{j,n}^{\text{off}} \right)$ and $\widehat{W}_j \left(t_{j,n}^{\text{off}} \right)$, defined in the subsequent sections) is saved until $\mathcal{M}$ reenters $\mathcal{O}_j$ at a later time.

Under Assumptions 4.4 and 4.6, (4–9) can be rewritten as[1]

$$\dot{\eta}_{m/c_j}(t) = W_j^T \sigma_j(\eta, t) + \varepsilon_j(\eta, t) + f_j(\eta, t). \tag{4–11}$$

Let the object's state estimation error, denoted by $\widetilde{\eta}_{m/c_j}(t) \in \mathbb{R}^7$, be defined as

$$\widetilde{\eta}_{m/c_j}(t) \triangleq \eta_{m/c_j}(t) - \hat{\eta}_{m/c_j}(t), \tag{4–12}$$

where $\hat{\eta}_{m/c_j}(t) \in \mathbb{R}^7$ is the estimate of $\eta_{m/c_j}(t)$. Taking the time-derivative of (4–12) and substituting for (4–11) yields

$$\dot{\widetilde{\eta}}_{m/c_j}(t) = W_j^T \sigma_j(\eta, t) + \varepsilon_j(\eta, t) + f_j(\eta, t) - \dot{\hat{\eta}}_{m/c_j}(t), \tag{4–13}$$

where $\dot{\hat{\eta}}_{m/c_j}(t) \in \mathbb{R}^7$ is the pose estimator update law. Additionally, the NN weight estimation error, $\widetilde{W}_j(t) \in \mathbb{R}^{p \times 7}$, is defined as

$$\widetilde{W}_j(t) \triangleq W_j - \widehat{W}_j(t), \tag{4–14}$$

---

[1] For brevity, the functional dependencies for $\sigma_j \left(\eta_{m/c_j}(t), \eta_{c_j/G}(t) \right)$ and $\varepsilon_j \left(\eta_{m/c_j}(t), \eta_{c_j/G}(t) \right)$ have been simplified to $\sigma_j(\eta, t)$ and $\varepsilon_j(\eta, t)$, respectively.

where $\widehat{W}_j(t) \in \mathbb{R}^{p \times 7}$ is the estimate of the ideal weights. Taking the time-derivative of (4–14) yields

$$\dot{\widetilde{W}}_j(t) = -\dot{\widehat{W}}_j(t) \tag{4–15}$$

where $\dot{\widehat{W}}_j(t)$ is the weight estimator update law. Stacking the state and weight estimation errors (i.e., (4–12) and (4–14), respectively) result in the composite error vector, $\xi_j(t) \in \mathbb{R}^{7+7p}$, which is defined as $\xi_j(t) \triangleq \begin{bmatrix} \widetilde{\eta}_{m/c_j}^T(t) & \text{vec}\left(\widetilde{W}_j(t)\right)^T \end{bmatrix}^T$, where the vec $(\cdot)$ operator denotes a stack of the columns of $(\cdot)$. Using the definition for $\xi_j(t)$, the estimation objective is to design $\dot{\hat{\eta}}_{m/c_j}(t)$ and $\dot{\widehat{W}}_j(t)$ such that $\xi_j(t) \in \mathcal{L}_\infty$.

4.2.1   State Estimator and Predictor - Update Law

Based on the subsequent stability analysis, the pose estimator (i.e., when $\sigma_j^f(t) = a$) and predictor (i.e., when $\sigma_j^f(t) = u$) update laws are designed as

$$\dot{\hat{\eta}}_{m/c_j}(t) = \begin{cases} \widehat{W}_j^T(t)\sigma_j(\eta, t) + f_j(\eta, t) + k_2\widetilde{\eta}_{m/c_j}(t) + k_3\text{sgn}\left(\widetilde{\eta}_{m/c_j}(t)\right), & \sigma_j^f = a \\ \text{proj}\left(\widehat{W}_j^T(t)\hat{\sigma}_j(\eta, t) + \hat{f}_j(\eta, t)\right), & \sigma_j^f = u \end{cases} \tag{4–16}$$

where $k_2, k_3 \in \mathbb{R}_{>0}$ are constant control gains, proj $(\cdot)$ is a smooth projection operator (see [28, Remark 3.7]) with state and velocity bounds which are known under Assumptions 4.4 and 3.3, $\hat{\sigma}_j(\eta, t) \triangleq \sigma_j\left(\hat{\eta}_{m/c_j}(t), \eta_{c_j/G}(t)\right)$, and $\hat{f}_j(\eta, t) \triangleq f_j\left(\hat{\eta}_{m/c_j}(t), \eta_{c_j/G}(t)\right)$. Substituting (4–16) into (4–13) yields the closed-loop error system

$$\dot{\widetilde{\eta}}_{m/c_j}(t) = \begin{cases} \widetilde{W}_j^T\sigma_j(\eta, t) + \varepsilon_j(\eta, t) - k_2\widetilde{\eta}_{m/c_j}(t) - k_3\text{sgn}\left(\widetilde{\eta}_{m/c_j}(t)\right), & \sigma_j^f = a \\ \widetilde{W}_j^T(t)\sigma_j(\eta, t) + \widehat{W}_j^T(t)\widetilde{\sigma}_j(\eta, t) + \varepsilon_j(\eta, t) + \widetilde{f}_j(\eta, t), & \sigma_j^f = u \end{cases} \tag{4–17}$$

where $\widetilde{\sigma}_j(\eta, t) \triangleq \sigma_j(\eta, t) - \hat{\sigma}_j(\eta, t)$, and $\widetilde{f}_j(\eta, t) \triangleq f_j(\eta, t) - \hat{f}_j(\eta, t)$.

4.2.2 Parameter Weight Estimator and Predictor - Update Law

Based on the subsequent stability analysis, the ideal weight estimator (i.e., when $\sigma_j^f(t) = a$) and predictor (i.e., when $\sigma_j^f(t) = u$) update laws are designed as

$$\dot{\widehat{W}}_j(t) = \begin{cases} \text{proj}\left(\Gamma \sigma_j(\eta, t) \tilde{\eta}_{m/c_j}^T(t) \right. \\ \left. + k_{CL}\Gamma\alpha \sum\limits_{i=1}^{N} \mathcal{Y}_{j,i}^T \left(\Delta\eta_{j,i}^T - \mathcal{F}_{j,i} - \mathcal{Y}_{j,i}\widehat{W}_j(t)\right) \right. \\ \left. + k_{CL}\Gamma\beta \sum\limits_{k=1}^{N} Y_{j,k}^T \left(\dot{\eta}_{j,k}^T - f_{j,k} - Y_{j,k}\widehat{W}_j(t)\right)\right), & \sigma_j^f = a \\ \text{proj}\left(k_{CL}\Gamma\alpha \sum\limits_{i=1}^{N} \mathcal{Y}_{j,i}^T \left(\Delta\eta_{j,i}^T - \mathcal{F}_{j,i} - \mathcal{Y}_{j,i}\widehat{W}_j(t)\right) \right. \\ \left. + k_{CL}\Gamma\beta \sum\limits_{k=1}^{N} Y_{j,k}^T \left(\dot{\eta}_{j,k}^T - f_{j,k} - Y_{j,k}\widehat{W}_j(t)\right)\right), & \sigma_j^f = u \end{cases} \qquad (4\text{–}18)$$

where $k_{CL} \in \mathbb{R}_{>0}$ is a constant control gain, $\Gamma \in \mathbb{R}^{p \times p}$ is a constant, positive definite control gain, and $\beta \triangleq 1 - \alpha \in [0,1]$ and $\alpha \in [0,1]$ are tuning parameters that adjust how previously recorded pose data (i.e., $\Delta\eta_{j,i}$) and velocity data (i.e., $\dot{\eta}_{j,k}$) influence the performance of the ideal weight estimator and predictor. Additionally, $\mathcal{Y}_{j,i} \triangleq \mathcal{Y}_j(t_i)$ and $\Delta\eta_{j,i} \triangleq \Delta\eta_j(t_i)$ represent recorded pose data at $t_i \in [\Delta t, t]$, where $\mathcal{Y}_j(t) \triangleq \int_{t-\Delta t}^{t} \sigma_j^T\left(\eta_{m/c_j}(\tau), \eta_{c_j/G}(\tau)\right) d\tau$, $\Delta\eta_j(t) \triangleq \eta_{m/c_j}(t) - \eta_{m/c_j}(t - \Delta t)$, and $\Delta t \in \mathbb{R}_{>0}$ is an integration window. Also, $Y_{j,k} \triangleq Y_j(t_k)$ and $\dot{\eta}_{j,k} \triangleq \dot{\eta}_{m/c_j}(t_k)$ represent recorded velocity data at $t_k \in [0,t]$, where $Y_{j,k} \triangleq \sigma_j^T\left(\eta_{m/c_j}(t_k), \eta_{c_j/G}(t_k)\right)$.[2] Furthermore, $N \in \mathbb{Z}_{>p}$ represents the size of the history stacks, $\mathcal{F}_{j,i} \triangleq \mathcal{F}_j(t_i)$, where $\mathcal{F}_j(t) \triangleq \int_{t-\Delta t}^{t} f_j^T\left(\eta_{m/c_j}(\tau), \eta_{c_j/G}(\tau)\right) d\tau$, and $f_{j,k} \triangleq f_j^T\left(\eta_{m/c_j}(t_k), \eta_{c_j/G}(t_k)\right)$.

The following development aims to gain a deeper understanding of the history stacks and aid in the development of the closed-loop error systems for the ideal weight

---

[2] The i, k indices in $\Delta\eta_{j,i}$ and $\dot{\eta}_{j,k}$ are not necessarily the same (i.e., the recorded data in the history stacks may be updated asynchronously).

estimator and predictor. For the pose data history stack, taking the transpose of (4–11), integrating over the time interval $[t - \Delta t,\, t]$, and evaluating at $t = t_i$ yields

$$\Delta \eta_{j,i}^T = \mathcal{Y}_{j,i} W_j + \mathcal{E}_{j,i} + \mathcal{F}_{j,i}, \qquad (4\text{–}19)$$

where $\mathcal{E}_{j,i} \triangleq \mathcal{E}_j(t_i)$ and $\mathcal{E}_j(t) \triangleq \int_{t-\Delta t}^{t} \varepsilon_j^T \left(\eta_{m/c_j}(\tau), \eta_{c_j/G}(\tau) \right) d\tau$. For the velocity data history stack, taking the transpose of (4–11) and evaluating at $t = t_k$ yields

$$\dot{\eta}_{j,k}^T = Y_{j,k} W_j + \varepsilon_{j,k} + f_{j,k}, \qquad (4\text{–}20)$$

where $\varepsilon_{j,k} \triangleq \varepsilon_j^T \left(\eta_{m/c_j}(t_k), \eta_{c_j/G}(t_k) \right)$. Substituting (4–19) and (4–20) into (4–18), yields a simplified expression for (4–18) that can then be substituted into (4–15) to yield the closed-loop error system for the weight estimator and predictor, described by

$$\dot{\widetilde{W}}_j(t) = \begin{cases} -\mathsf{proj}\left(\Gamma \sigma_j(\eta, t) \tilde{\eta}_{m/c_j}^T(t) + k_{CL} \Gamma \Psi_j(t) \widetilde{W}_j(t) \right. \\ \left. + k_{CL} \Gamma \alpha \sum\limits_{i=1}^{N} \mathcal{Y}_{j,i}^T \mathcal{E}_{j,i} + k_{CL} \Gamma \beta \sum\limits_{k=1}^{N} Y_{j,k}^T \varepsilon_{j,k} \right), & \sigma_j^f = a \\ -\mathsf{proj}\left(k_{CL} \Gamma \Psi_j(t) \widetilde{W}_j(t) \right. \\ \left. + k_{CL} \Gamma \alpha \sum\limits_{i=1}^{N} \mathcal{Y}_{j,i}^T \mathcal{E}_{j,i} + k_{CL} \Gamma \beta \sum\limits_{k=1}^{N} Y_{j,k}^T \varepsilon_{j,k} \right), & \sigma_j^f = u \end{cases} \qquad (4\text{–}21)$$

where $\Psi_j(t) \triangleq \alpha \sum\limits_{i=1}^{N} \mathcal{Y}_{j,i}^T \mathcal{Y}_{j,i} + \beta \sum\limits_{k=1}^{N} Y_{j,k}^T Y_{j,k}$ represents the composite history stack.

4.3 Analysis

As the target agent travels across the target tracking environment, it transitions between being inside and outside the FOV of the camera network, causing periods when measurement feedback is available (i.e., $\sigma_j^f(t) = a$) and unavailable (i.e., $\sigma_j^f(t) = u$). When $\sigma_j^f(t) = a$, the estimator in (4–16) and (4–18) is active. The time spent in the $\sigma_j^f(t) = a$ subsystem is denoted by $\Delta t_{j,n}^{\mathsf{on}} \triangleq t_{j,n}^{\mathsf{off}} - t_{j,n}^{\mathsf{on}}$, where $t_{j,n}^{\mathsf{on}}$ and $t_{j,n}^{\mathsf{off}}$ represent the nth time instance when feedback first became available and unavailable

while $\mathcal{M} \subset \mathcal{O}_j$, respectively. When $\sigma_j^f(t) = u$, the predictor in (4–16) and (4–18) is active. Two scenarios can cause $\sigma_j^f(t) = u$, which influences the definition for the time spent in the $\sigma_j^f(t) = u$ subsystem, denoted by $\Delta t_{j,n}^{\text{off}}$. First, feedback loss for $\mathcal{M}$ can occur when $\mathcal{M}$ is transitioning between $\mathcal{O}_j$ and $\mathcal{O}_{j+1}$ (i.e., $\mathcal{M} \subset \mathcal{O}_C^c$), resulting in $\Delta t_{j,n}^{\text{off}} \triangleq t_{j+1,n}^{\text{on}} - t_{j,n}^{\text{off}}$, where $t_{j+1,n}^{\text{on}}$ represents the time instance when feedback first becomes available when $\mathcal{M} \subset \mathcal{O}_{j+1}$ (i.e., $\sigma_{j+1}^f(t) = a$). Second, feedback loss for $\mathcal{M}$ can occur when $\mathcal{M}$ is occluded by an unknown object in $\mathcal{O}_j$ (i.e, $\mathcal{M} \subset \mathcal{O}_j \wedge \mathcal{M} \notin \mathcal{F}_{c_j}$), resulting in $\Delta t_{j,n}^{\text{off}} \triangleq t_{j,n+1}^{\text{on}} - t_{j,n}^{\text{off}}$, where $t_{j,n+1}^{\text{on}}$ represents the next time instance (i.e., $n + 1$) when feedback is available while $\mathcal{M} \subset \mathcal{O}_j$ (i.e., $\sigma_j^f(t) = a$). Thus, the $j + 1$ index increase indicates that $\mathcal{M}$ has transitioned between operating regions in $\mathcal{O}_C$, while the $n + 1$ index increase indicates that $\mathcal{M}$ is occluded by an unknown object in $\mathcal{O}_j$. The subsequent analysis considers both cases, but emphasis is placed on $\mathcal{M}$ transitioning between operating regions in $\mathcal{O}_C$. Furthermore, due to the CCL adaptation technique used in (4–18), the $\sigma_j^f(t) = a$ subsystem is further partitioned into two modes. Let $\sigma_j^d(t) \in \{a, u\}$ be a switching signal indicating whether the composite history stack (i.e., $\Psi_j(t)$) satisfies (i.e., $T_j \in [t_{j,n}^{\text{on}}, t_{j,n}^{\text{off}}) \wedge \sigma_j^d(t) = a$) or does not satisfy (i.e., $T_j \notin [t_{j,n}^{\text{on}}, t_{j,n}^{\text{off}}) \wedge \sigma_j^d(t) = u$) the finite excitation condition in Assumption 4.7.

Assumption 4.7. At time $T_j \in \mathbb{R}_{>0}$, there exists a constant $\underline{\lambda} \in \mathbb{R}_{>0}$ such that

$\forall t \geq T_j, \; \lambda_{\min}\{\Psi_j(t)\} \geq \underline{\lambda}, \;\;$ where $\lambda_{\min}\{\cdot\}$ refers to the minimum eigenvalue of $\{\cdot\}$ (see [24] and [4]).

The first instance when $\sigma_j^f(t) = a$, $\Psi_j(t)$ contains insufficient excitation data and the finite excitation condition in Assumption 4.7 is not met. The lack of sufficient excitation data reduces the performance of the estimator, however as shown in Lemma 4.2, the estimator remains bounded. As $\Psi_j(t)$ is populated with new data, techniques like the singular value maximization algorithm in [29] and [31] can be used to add and remove data to maximize the minimum eigenvalue of $\Psi_j(t)$. After a finite period of time, $\Psi_j(t)$ is populated with sufficient data and the finite excitation condition is met at T_j, improving

the performance of the estimator, as shown in Lemma 4.2. Furthermore, the data collected when $\sigma_j^f(t) = a$ is also used in the predictor, when $\sigma_j^f(t) = u$.

The Lyapunov-based analyses in the subsequent sections utilize the Lyapunov function candidates

$$V_j^C\left(\zeta_j\left(t\right)\right) \triangleq \frac{1}{2}\widetilde{\eta}_{c_j/G}^T\left(t\right)\widetilde{\eta}_{c_j/G}\left(t\right), \tag{4–22}$$

$$V_j^M\left(\xi_j\left(t\right)\right) \triangleq \frac{1}{2}\widetilde{\eta}_{m/c_j}^T\left(t\right)\widetilde{\eta}_{m/c_j}\left(t\right) + \frac{1}{2}\text{tr}\left(\widetilde{W}_j^T\left(t\right)\Gamma^{-1}\widetilde{W}_j\left(t\right)\right), \tag{4–23}$$

where $V_j^C : \mathbb{R}^7 \to \mathbb{R}_{\geq 0}$ is used for the controller, and $V_j^M : \mathbb{R}^{7+7p} \to \mathbb{R}_{\geq 0}$ is used for the estimator and predictor, respectively. To facilitate the stability analysis for the estimator and predictor, (4–23) can be bounded by $\frac{1}{2}\gamma_1 \left\|\xi_j\left(t\right)\right\|^2 \leq V_j^M\left(\xi_j\left(t\right)\right) \leq \frac{1}{2}\gamma_2 \left\|\xi_j\left(t\right)\right\|^2$, where $\gamma_1 \triangleq \min\{1, \lambda_{\min}\{\Gamma^{-1}\}\}$, $\gamma_2 \triangleq \max\{1, \lambda_{\max}\{\Gamma^{-1}\}\}$, $\lambda_{\max}\{\cdot\}$ refers to the maximum eigenvalue of $\{\cdot\}$, and $\min\{\cdot\}$ and $\max\{\cdot\}$ returns the minimum and maximum value in the set $\{\cdot\}$, respectively. Additionally, because of the projection operator in (4–16) and (4–18), $\widehat{W}_j\left(t\right) \leq \left\|\widehat{W}_j\left(t\right)\right\| \leq \dot{\eta}_{\max}$, where $\dot{\eta}_{\max} \in \mathbb{R}$ denotes a known bounding constant via Assumptions 4.7. Also, $\|W_j\| \leq \dot{\eta}_{\max}$, resulting in $\widetilde{W}_j\left(t\right) \leq \left\|\widetilde{W}_j\left(t\right)\right\| \leq 2\dot{\eta}_{\max}$. Using these bounds, $V_j^M\left(\xi_j\left(t\right)\right) \leq \frac{1}{2}\left\|\tilde{\eta}_{m/c_j}\left(t\right)\right\|^2 + c_2$, where $c_2 \triangleq 2\lambda_{\max}\{\Gamma^{-1}\}\dot{\eta}_{\max}^2 \in \mathbb{R}_{>0}$ is a constant. Taking the time-derivative of (4–22) yields

$$\dot{V}_j^C\left(\zeta_j\left(t\right)\right) = \widetilde{\eta}_{c_j/G}^T\left(t\right)\dot{\widetilde{\eta}}_{c_j/G}\left(t\right). \tag{4–24}$$

Additionally, taking the time-derivative of (4–23) yields

$$\dot{V}_j^M\left(\xi_j\left(t\right)\right) = \widetilde{\eta}_{m/c_j}^T\left(t\right)\dot{\widetilde{\eta}}_{m/c_j}\left(t\right) + \text{tr}\left(\widetilde{W}_j^T\left(t\right)\Gamma^{-1}\dot{\widetilde{W}}_j\left(t\right)\right). \tag{4–25}$$

4.3.1 Controller - Stability Analysis

Lemma 4.1. *For the jth operating region (i.e., $\mathcal{O}_j$), the controller in (4–6) remains bounded for $t \in [t_j^{on}, \infty)$, where t_j^{on} represents the first time instance when the controller becomes active for $\mathcal{O}_j$.*

Proof. Substituting the closed-loop error system (4–7) into (4–24) and simplifying yields

$$\dot{V}_j^C\left(\zeta_j\left(t\right)\right) \leq -k_1 \widetilde{\eta}_{c_j/G}^T\left(t\right)\widetilde{\eta}_{c_j/G}\left(t\right). \tag{4–26}$$

Using the definition in (4–22), (4–26) can be rewritten in terms of $V_j^C\left(\zeta_j\left(t\right)\right)$, yielding

$$\dot{V}_j^C\left(\zeta_j\left(t\right)\right) \leq -2k_1 V_j^C\left(\zeta_j\left(t\right)\right).$$

Solving the first-order linear ordinary differential equation yields

$$V_j^C\left(\zeta_j\left(t\right)\right) \leq V_j^C\left(\zeta_j\left(t_j^{on}\right)\right)\exp\left[-\lambda_D^C\left(t - t_j^{on}\right)\right], \tag{4–27}$$

where $\lambda_D^C \triangleq 2k_1 \in \mathbb{R}_{>0}$ is a known constant. $\qquad\square$

4.3.2 Estimator and Predictor - Stability Analysis

Lemma 4.2. *For the jth operating region, both the estimator in (4–16) and (4–18) when $t \in [t_{j,n}^{on}, t_{j,n}^{off})$, and the predictor in (4–16) and (4–18) when $t \in [t_{j,n}^{off}, t_{j+1,n}^{on})$ or $t \in [t_{j,n}^{off}, t_{j,n+1}^{on})$, remain bounded.*

Proof. Substituting the closed-loop error systems (4–17) and (4–21) into (4–25) and simplifying yields

$$\dot{V}_j^M\left(\xi_j\left(t\right)\right) \leq \begin{cases} -k_2\left\|\tilde{\eta}_{m/c_j}\left(t\right)\right\|^2 + c_1, & \sigma_j^f = a \wedge \sigma_j^d = u \\ -\min\left\{k_2, \lambda_{CL}\right\}\left\|\xi_j\left(t\right)\right\|^2 + c_1, & \sigma_j^f = a \wedge \sigma_j^d = a \\ \frac{1}{2}\left\|\xi_j\left(t\right)\right\|^2 + c_3, & \sigma_j^f = u \end{cases} \tag{4–28}$$

where $c_1 \triangleq 2k_{CL}N\dot{\eta}_{\max}\bar{\varepsilon}\left(\alpha\Delta t + 1 - \alpha\right) \in \mathbb{R}_{>0}$, $\lambda_{CL} \triangleq k_{CL}\lambda_{\min}\left\{\Psi_j\left(t\right)\right\} \in \mathbb{R}_{>0}$, and $c_3 \triangleq \frac{1}{2}\left(6\dot{\eta}_{\max} + \bar{\varepsilon}\right)^2 + c_1 \in \mathbb{R}_{>0}$ are known constants, and $k_3 > \bar{\varepsilon}$. Using the bounds on (4–23), (4–28) can be rewritten in terms of $V_j^M\left(\xi_j\left(t\right)\right)$, yielding

$$
\dot{V}_j^M\left(\xi_j\left(t\right)\right) \leq
\begin{cases}
-\lambda_D^M V_j^M\left(\xi_j\left(t\right)\right) + 2k_2 c_2 + c_1, & \sigma_j^f = a \wedge \sigma_j^d = u \\
-\lambda_{D,T}^M V_j^M\left(\xi_j\left(t\right)\right) + c_1, & \sigma_j^f = a \wedge \sigma_j^d = a \\
\lambda_G^M V_j^M\left(\xi_j\left(t\right)\right) + c_3, & \sigma_j^f = u
\end{cases}
\tag{4–29}
$$

where $\lambda_D^M \triangleq 2k_2 \in \mathbb{R}_{>0}$, $\lambda_{D,T}^M \triangleq \frac{2\min\{k_2, \lambda_{CL}\}}{\max\{1, \lambda_{\max}\{\Gamma^{-1}\}\}} \in \mathbb{R}_{>0}$, and $\lambda_G^M \triangleq \frac{1}{\min\{1, \lambda_{\min}\{\Gamma^{-1}\}\}} \in \mathbb{R}_{>0}$ are known constants. Solving the first-order linear ordinary differential equations in (4–29) yields

$$
V_j^M\left(\xi_j\left(t\right)\right) \leq
\begin{cases}
V_j^M\left(\xi_j\left(t_{j,n}^{\mathsf{on}}\right)\right)\exp\left[-\lambda_D^M(t - t_{j,n}^{\mathsf{on}})\right] + \beta_1, & \sigma_j^f = a \wedge \sigma_j^d = u \\
V_j^M\left(\xi_j\left(t_{j,n}^{\mathsf{on}}\right)\right)\exp\left[-\lambda_{D,T}^M\left(t - t_{j,n}^{\mathsf{on}}\right)\right] + c_{UB}, & \sigma_j^f = a \wedge \sigma_j^d = a \\
V_j^M\left(\xi_j\left(t_{j,n}^{\mathsf{off}}\right)\right)\exp\left[\lambda_G^M\left(t - t_{j,n}^{\mathsf{off}}\right)\right], & \sigma_j^f = u
\end{cases}
\tag{4–30}
$$

where $c_{UB} \triangleq \frac{c_1\max\{1, \lambda_{\max}\{\Gamma^{-1}\}\}}{2\min\{k_2, \lambda_{CL}\}} \in \mathbb{R}_{>0}$ and $\beta_1 \triangleq \frac{c_1}{2k_2} + c_2 \in \mathbb{R}_{>0}$ are known constants. $\qquad\square$

4.3.3 Dwell-Time Analysis

Theorem 4.1. *For the jth operating region, the proposed estimator and predictor remain bounded for $t \in [t_{j,n}^{\mathsf{on}}, t_{j+1,n}^{\mathsf{on}})$, provided*

$$
\Delta t_{j,n}^{\mathit{off}} \leq
\begin{cases}
\frac{1}{\lambda_G^M}\ln\left(\overline{V}\left(\overline{V}\nu_1 + \beta_1\right)^{-1}\right), & \sigma_j^d = u \\
\frac{1}{\lambda_G^M}\ln\left(\overline{V}\left(\overline{V}\nu_2 + \beta_1\nu_3 + c_{UB}\right)^{-1}\right), & \sigma_j^d = a \wedge \sigma_j^h = u \\
\frac{1}{\lambda_G^M}\ln\left(\overline{V}\left(\overline{V}\nu_4 + c_{UB}\right)^{-1}\right), & \sigma_j^d = a \wedge \sigma_j^h = a
\end{cases}
\tag{4–31}
$$

where $\overline{V} \in \mathbb{R}_{>0}$ represents the maximum allowable value that $V_j^M\left(\xi_j\left(t\right)\right)$ may grow during the period when $t \in [t_{j,n}^{\mathsf{on}}, t_{j+1,n}^{\mathsf{on}})$, $\sigma_j^h\left(t\right) \triangleq \{a, u\}$ is a switching signal indicating

whether $T_j \in [t_{j,n}^{\text{on}}, t_{j,n}^{\text{off}})$ *(i.e.,* $\sigma_j^h(t) = u$ *) or* $T_j \in [t_{j,n-q}^{\text{on}}, t_{j,n-q}^{\text{off}})$ *(i.e.,* $\sigma_j^h(t) = a$*),*

$q \in \{1, \ldots, n-1\}$*, and* $\nu_1, \nu_2, \nu_3, \nu_4 \in \mathbb{R}_{>0}$ *are known constants after* $t_{j,n}^{\text{off}}$.

Remark 4.3. If $V_j^M(\xi_j(t))$ exceeds $\overline{V}$, the uncertainty on $\eta_{m/c_j}(t)$ may grow larger than $\mathcal{V}_{c_j}$, making the tracking objective impractical. Hence, the value of $\overline{V}$ is dictated by the camera parameters that influence $\mathcal{V}_{c_j}$ and the pose of $\mathcal{C}_j$. Additionally, after the composite history stack (i.e., $\Psi_j(t)$) satisfies the finite excitation condition in Assumption 4.7 (i.e., $\sigma_j^d(t) = a$), the maximum time $\mathcal{M}$ may stay outside of a feedback region (i.e., $\Delta t_{j,n}^{\text{off}}$) increases as indicated in (4–31). Also, $\Delta t_{j,n}^{\text{off}}$ further increases if $\mathcal{M}$ reenters an operating region (e.g., $\mathcal{O}_j$) where the finite excitation condition has already been met in a previous n cycle for $\mathcal{O}_j$ (i.e., $\sigma_j^h(t) = a$). Furthermore, Theorem 4.1 demonstrates that the proposed framework remains bounded for $t \in [t_{j,n}^{\text{on}}, t_{j+1,n}^{\text{on}})$ (i.e., feedback loss caused by $\mathcal{M}$ leaving $\mathcal{O}_j$, traveling through $\mathcal{O}_C^c$, and entering $\mathcal{O}_{j+1}$). However, Theorem 4.1 can be directly extended for $t \in [t_{j,n}^{\text{on}}, t_{j,n+1}^{\text{on}})$ (i.e., feedback loss caused by $\mathcal{M}$ being occluded by an object in $\mathcal{O}_j$ while $\mathcal{M} \subset \mathcal{O}_j$), and will result in (4–31).

Proof. The objective of this analysis is to show that

$$V_j^M\left(\xi_j\left(t_{j+1,n}^{\text{on}}\right)\right) \leq \overline{V}.$$

Using the $\sigma_j^f(t) = u$ case in (4–30), $V_j^M\left(\xi_j\left(t_{j+1,n}^{\text{on}}\right)\right)$ can be bounded by

$$V_j^M\left(\xi_j\left(t_{j+1,n}^{\text{on}}\right)\right) \leq V_j^M\left(\xi_j\left(t_{j,n}^{\text{off}}\right)\right) \exp\left[\lambda_G^M \Delta t_{j,n}^{\text{off}}\right] \leq \overline{V}. \tag{4–32}$$

The $V_j^M\left(\xi_j\left(t_{j,n}^{\text{off}}\right)\right)$ term in (4–32) can be bounded by three equations depending if the composite history stack (i.e., $\Psi_j(t)$) satisfies the finite excitation condition in Assumption 4.7 (i.e., $\sigma_j^d(t) = u$ or $\sigma_j^d(t) = a$). Consider the first case where $\sigma_j^d(t) = u$, evaluating the $\sigma_j^f(t) = a \wedge \sigma_j^d(t) = u$ case in (4–30) at $t_{j,n}^{\text{off}}$ allows $V_j^M\left(\xi_j\left(t_{j,n}^{\text{off}}\right)\right)$ to be bounded by

$$V_j^M\left(\xi_j\left(t_{j,n}^{\text{off}}\right)\right) \leq V_j^M\left(\xi_j\left(t_{j,n}^{\text{on}}\right)\right)\nu_1 + \beta_1,$$

where $\nu_1 \triangleq \exp\left[-\lambda_D^M \Delta t_{j,n}^{\text{on}}\right] \in \mathbb{R}_{>0}$. Consider the second case where $\sigma_j^d(t) = a$ and $T_j \in [t_{j,n}^{\text{on}}, t_{j,n}^{\text{off}})$ (i.e., $\sigma_j^h(t) = u$), first the $\sigma_j^f(t) = a \wedge \sigma_j^d(t) = a$ case in (4–30) is evaluated at $t_{j,n}^{\text{off}}$ with an initial condition of T_j instead of $t_{j,n}^{\text{on}}$, then the $\sigma_j^f(t) = a \wedge \sigma_j^d(t) = u$ case in (4–30) is evaluated at T_j. Combining the results of these operations allows $V_j^M\left(\xi_j\left(t_{j,n}^{\text{off}}\right)\right)$ to be bounded by

$$V_j^M\left(\xi_j\left(t_{j,n}^{\text{off}}\right)\right) \leq V_j^M\left(\xi_j\left(t_{j,n}^{\text{on}}\right)\right)\nu_2 + \beta_1\nu_3 + c_{UB},$$

where $\nu_2 \triangleq \exp\left[-\lambda_D^M \Delta t_{j,n,I}^{\text{on}} - \lambda_{D,T}^M \Delta t_{j,n,S}^{\text{on}}\right] \in \mathbb{R}_{>0}$, $\nu_3 \triangleq \exp\left[-\lambda_{D,T}^M \Delta t_{j,n,S}^{\text{on}}\right] \in \mathbb{R}_{>0}$, and $\Delta t_{j,n,I}^{\text{on}} \triangleq T_j - t_{j,n}^{\text{on}}$ and $\Delta t_{j,n,S}^{\text{on}} \triangleq t_{j,n}^{\text{off}} - T_j$ represent the length of time when the excitation data in $\Psi_j(t)$ was insufficiently and sufficiently rich during cycle n for $\mathcal{O}_j$, respectively. Additionally, summing $\Delta t_{j,n,I}^{\text{on}}$ and $\Delta t_{j,n,S}^{\text{on}}$ yields $\Delta t_{j,n}^{\text{on}}$. Now, if $\mathcal{M}$ reenters $\mathcal{O}_j$ where the finite excitation condition for $\Psi_j(t)$ was satisfied in a previous n cycle (i.e., $\sigma_j^d(t) = a$ and $\sigma_j^h(t) = a$), the $\sigma_j^f(t) = a \wedge \sigma_j^d(t) = a$ case in (4–30) is evaluated at $t_{j,n}^{\text{off}}$ allows $V_j^M\left(\xi_j\left(t_{j,n}^{\text{off}}\right)\right)$ to be bounded by

$$V_j^M\left(\xi_j\left(t_{j,n}^{\text{off}}\right)\right) \leq V_j^M\left(\xi_j\left(t_{j,n}^{\text{on}}\right)\right)\nu_4 + c_{UB},$$

where $\nu_4 \triangleq \exp\left[-\lambda_{D,T}^M \Delta t_{j,n}^{\text{on}}\right] \in \mathbb{R}_{>0}$. Compiling the three cases for the bounds on $V_j^M\left(\xi_j\left(t_{j,n}^{\text{off}}\right)\right)$ yields

$$V_j^M\left(\xi_j\left(t_{j,n}^{\text{off}}\right)\right) \leq \begin{cases} V_j^M\left(\xi_j\left(t_{j,n}^{\text{on}}\right)\right)\nu_1 + \beta_1, & \sigma_j^d = u \\ V_j^M\left(\xi_j\left(t_{j,n}^{\text{on}}\right)\right)\nu_2 + \beta_1\nu_3 + c_{UB}, & \sigma_j^d = a \wedge \sigma_j^h = u \\ V_j^M\left(\xi_j\left(t_{j,n}^{\text{on}}\right)\right)\nu_4 + c_{UB}, & \sigma_j^d = a \wedge \sigma_j^h = a. \end{cases} \quad (4\text{–}33)$$

Substituting (4–33) into (4–32) and upper bounding $V_j^M\left(\xi_j\left(t_{j,n}^{\text{on}}\right)\right)$ by $\overline{V}$ (i.e., the previous feedback cycle n for $\mathcal{O}_j$ is also bounded by $\overline{V}$) yields

$$\overline{V} \geq \begin{cases} \left(\overline{V}\nu_1 + \beta_1\right) \exp\left[\lambda_G^M \Delta t_{j,n}^{\text{off}}\right], & \sigma_j^d = u \\ \left(\overline{V}\nu_2 + \beta_1\nu_3 + c_{UB}\right) \exp\left[\lambda_G^M \Delta t_{j,n}^{\text{off}}\right], & \sigma_j^d = a \wedge \sigma_j^h = u \\ \left(\overline{V}\nu_4 + c_{UB}\right) \exp\left[\lambda_G^M \Delta t_{j,n}^{\text{off}}\right], & \sigma_j^d = a \wedge \sigma_j^h = a. \end{cases} \quad (4\text{--}34)$$

Solving (4–34) for $\Delta t_{j,n}^{\text{off}}$ yields (4–31). $\qquad\qquad\qquad\qquad\qquad \square$

Theorem 4.2. *After the dwell-time condition for $\Delta t_{j,n}^{\text{off}}$ is satisfied and $\mathcal{M}$ enters the FOV (i.e., $\mathcal{F}_{c_{j+1}}$) belonging to the neighboring operating region (i.e., $\mathcal{O}_{j+1}$), a new feedback cycle begins and the estimator in (4–16) and (4–18) will be bounded by $\underline{V}$, provided*

$$\Delta t_{j+1,n}^{on} \geq \begin{cases} -\frac{1}{\lambda_D^M}\ln\left(\left(\underline{V} - \beta_1\right)\overline{V}^{-1}\right), & \sigma_j^h = u \\ -\frac{1}{\lambda_{D,T}^M}\ln\left(\left(\underline{V} - c_{UB}\right)\overline{V}^{-1}\right), & \sigma_j^h = a \end{cases} \quad (4\text{--}35)$$

where $\underline{V} \in \mathbb{R}_{>0}$ represents the threshold that $V_{j+1}^M\left(\xi_{j+1}\left(t\right)\right)$ must decay below during the period then $t \in [t_{j+1,n}^{\text{on}}, t_{j+1,n}^{\text{off}})$.

Remark 4.4. The design of $\underline{V}$ can be considered an engineering parameter, that is dependent on the configuration of $\mathcal{O}_C$, the camera parameters that influence $\mathcal{V}_{c_j}$, the pose of $\mathcal{C}_j$, and assumptions made about the target (e.g., $\dot{\eta}_{\max}$). If feedback loss was a result of an unknown object occluding $\mathcal{M}$ when $\mathcal{M} \subset \mathcal{O}_j$, Theorem 4.2 can be directly extended for $t \in [t_{j,n+1}^{\text{on}}, t_{j,n+1}^{\text{off}})$, which will result in (4–35), but for $\Delta t_{j,n+1}^{\text{on}}$.

Proof. The objective of this analysis is to show that

$$V_{j+1}^M\left(\xi_{j+1}\left(t_{j+1,n}^{\text{off}}\right)\right) \leq \underline{V}.$$

First, the analysis considers the case where either $\mathcal{M}$ enters $\mathcal{O}_{j+1}$ for the first time or $\mathcal{M}$ reenters $\mathcal{O}_{j+1}$, however the finite excitation condition in Assumption 4.7 was not met during the previous instance when $\mathcal{M} \subset \mathcal{O}_{j+1}$ (i.e., $\sigma_j^h\left(t\right) = u$). Second, the analysis considers the case when $\mathcal{M}$ reenters $\mathcal{O}_{j+1}$ and the finite excitation condition was met during a previous instance when $\mathcal{M} \subset \mathcal{O}_{j+1}$ (i.e., $\sigma_j^h\left(t\right) = a$). For the $\sigma_j^h\left(t\right) = u$ case,

the $\sigma_j^f(t) = a \wedge \sigma_j^d(t) = u$ case for (4–30) is evaluated at $t_{j+1,n}^{\text{off}}$ and $V_{j+1}^M\left(\xi_{j+1}\left(t_{j+1,n}^{\text{on}}\right)\right)$ is upper bounded by $\overline{V}$, yielding

$$\overline{V}\exp\left[-\lambda_D^M\Delta t_{j+1,n}^{\text{on}}\right] + \beta_1 \leq \underline{V}.$$

Similarly, for the $\sigma_j^h(t) = a$ case, the $\sigma_j^f(t) = a \wedge \sigma_j^d(t) = a$ case for (4–30) is evaluated at $t_{j+1,n}^{\text{off}}$ and $V_{j+1}^M\left(\xi_{j+1}\left(t_{j+1,n}^{\text{on}}\right)\right)$ is upper bounded by $\overline{V}$, yielding

$$\overline{V}\exp\left[-\lambda_{D,T}^M\Delta t_{j+1,n}^{\text{on}}\right] + c_{UB} \leq \underline{V}.$$

Compiling the two cases for the bounds on $V_{j+1}^M\left(\xi_{j+1}\left(t_{j+1,n}^{\text{off}}\right)\right)$ yields

$$\underline{V} \geq \begin{cases} \overline{V}\exp\left[-\lambda_D^M\Delta t_{j+1,n}^{\text{on}}\right] + \beta_1, & \sigma_j^h = u \\ \overline{V}\exp\left[-\lambda_{D,T}^M\Delta t_{j+1,n}^{\text{on}}\right] + c_{UB}, & \sigma_j^h = a. \end{cases} \qquad (4\text{–}36)$$

Solving (4–36) for $\Delta t_{j+1,n}^{\text{on}}$ yields (4–35). $\qquad\square$

CHAPTER 5
CONCLUSIONS

In Chapter 3, an estimator and predictor are developed for approximating the pose and velocity of a moving target, using a sparsely distributed network of stationary cameras. The sparsity of the camera network is meant to maximize the observable area for a given environment by not requiring overlapping FOVs for the entire camera network. When tracking a target using a sparse camera network, there are periods when measurement feedback is not available for the target. While feedback is available, measurements of the target's state are recorded and used to approximate the target's motion model. This motion model is then used in a predictor, when feedback is not available, to propagate the target's state estimate into the non-feedback regions. Using a Lyapunov-based switched systems approach, the proposed framework developed in Chapter 3 is proven to remain bounded provided the dwell-time conditions are satisfied. These dwell-time conditions provide a metric for how long the target may travel outside the feedback regions, and for how long measurements are required when in the feedback regions. Moreover, an error growth analysis was developed using these dwell-time conditions, which relates the error dynamics to the physical network configuration.

In Chapter 4, a controller, estimator, and predictor framework is developed for estimating the pose and velocity states of a moving target, using a mobile network of cooperative agents, where the cooperative agents are constrained to be within non-overlapping operating regions. Since the operating regions are non-overlapping, periods exist when feedback of the target is unavailable. When the target is initially observed by a cooperative agent in the accompanying operating region, a controller is used to regulate the cooperative agent's pose to track the target, establishing visual feedback for the target while in the operating region. During this period, measurements of the target's pose and velocity state are recorded and used to approximate the target's

motion model. When feedback is not available, the approximated motion model is then used in a predictor to propagate the target's state estimates into the non-feedback regions, informing the cooperative agent in the neighboring operating region where to intercept the target. Using a Lyapunov-based switched systems approach, the proposed framework developed in Chapter 4 is proven to remain bounded, provided the developed minimum and maximum dwell-time conditions are satisfied. The maximum dwell-time condition offers an upper bound for the length of time that measurement feedback for the target can be unavailable, while considering the quality of the approximated motion model (i.e., via the minimum eigenvalue condition on the composite history stack), obtained when feedback was previously available. Through the design of $\overline{V}$, this dwell-time condition ensures that the target's positional uncertainty does not grow larger than the cooperative agent's FOV, ensuring that the tracking objective does not become impractical for future feedback cycles. Additionally, the minimum dwell-time condition offers a lower bound for the length of time that measurement feedback must be available. Through the design of $\underline{V}$, this dwell-time condition ensures that the estimator and controller used to approximate the target's motion model remains bounded for all feedback cycles.

The utility of the underlying estimator and predictor framework presented in this thesis is demonstrated by considering stationary and mobile networks of cooperative agents for tracking a moving target. The developments in Chapter 3 can be used to improve the the design of stationary camera networks by identifying areas of the network that may cause instabilities in the target's pose estimates, provided assumptions are made about the class of targets being tracked and their operating environments (e.g., vehicles traveling along a known road network). Additionally, the developments in Chapter 4 enables a mobile network of cooperative agents to intermittently track a moving target, reducing the quantity of agents needed for the tracking objective or

increasing the coverage area of the network. Future work will seek to validate the theoretical framework presented in this thesis through experiments, the framework will be adapted for non-holonomic systems, the time required to correctly identify a previously observed target will be considered, and methods for improving the performance of the framework, within the scope of this thesis, will be examined (e.g., the sharing of data and approximated motion models between operating regions). Additionally, future work will explore novel methods for further reducing the density of cooperative agents needed for the tracking objective. One possible method would be to allow the cooperative agents to momentarily leave their operating regions (i.e., the regions where state feedback is available) to continue tracking the target into the feedback-denied region, reducing the time the target remains unobserved. However, two significant challenges may arise. While a cooperative agent is operating in the feedback-denied region, estimates of the cooperative agent's pose may become unstable and an additional maximum dwell-time condition would be needed to ensure that the cooperative agent returns to its designated operating region. Also, instabilities in the cooperative agent's pose estimates may cause instabilities in the target's pose estimates, even if visual feedback for the target is available. Addressing these challenges may lead to a viable method for increasing the time the target may operate in the feedback-denied region, further reducing the density of cooperative agents needed for the tracking objective.

REFERENCES

[1] S. Avidan and A. Shashua, "Trajectory triangulation: 3D reconstruction of moving points from a monocular image sequence," *IEEE Trans. Pattern Anal. Mach. Intell.*, vol. 22, no. 4, pp. 348–357, Apr. 2000.

[2] J. Kaminski and M. Teicher, "A general framework for trajectory triangulation," *J. Math. Imag. Vis.*, vol. 21, no. 1, pp. 27–41, 2004.

[3] D. Chwa, A. Dani, and W. E. Dixon, "Range and motion estimation of a monocular camera using static and moving objects," *IEEE Trans. Control Syst. Tech.*, vol. 24, no. 4, pp. 1174–1183, July 2016.

[4] Z. Bell, P. Deptula, H.-Y. Chen, E. Doucette, and W. E. Dixon, "Velocity and path reconstruction of a moving object using a moving camera," in *Proc. Am. Control Conf.*, 2018, pp. 5256–5261.

[5] A. Parikh, T.-H. Cheng, R. Licitra, and W. E. Dixon, "A switched systems approach to image-based localization of targets that temporarily leave the camera field of view," *IEEE Trans. Control Syst. Technol.*, vol. 26, no. 6, pp. 2149–2156, 2018.

[6] A. Parikh, R. Kamalapurkar, and W. E. Dixon, "Target tracking in the presence of intermittent measurements via motion model learning," *IEEE Trans. Robot.*, vol. 34, no. 3, pp. 805–819, 2018.

[7] R. Hartley and A. Zisserman, *Multiple View Geometry in Computer Vision*. Cambridge University Press, 2003.

[8] Y. Ma, S. Soatto, J. Kosecka, and S. Sastry, *An Invitation to 3-D Vision*. Springer, 2004.

[9] A. Dani, N. Fischer, and W. E. Dixon, "Single camera structure and motion," *IEEE Trans. Autom. Control*, vol. 57, no. 1, pp. 241–246, Jan. 2012.

[10] V. Chitrakaran, D. M. Dawson, W. E. Dixon, and J. Chen, "Identification of a moving object's velocity with a fixed camera," *Automatica*, vol. 41, pp. 553–562, 2005.

[11] Z. I. Bell, H.-Y. Chen, A. Parikh, and W. E. Dixon, "Single scene and path reconstruction with a monocular camera using integral concurrent learning," in *Proc. IEEE Conf. Decis. Control*, 2017, pp. 3670–3675.

[12] Z. I. Bell, C. Harris, R. Sun, and W. E. Dixon, "Structure and velocity estimation of a moving object via synthetic persistence by a network of stationary cameras," in *Proc. IEEE Conf. Decis. Control*, Nice, Fr, Dec. 2019.

[13] M. W. M. G. Dissanayake, P. Newman, S. Clark, H. F. Durrant-Whyte, and M. Csorba, "A solution to the simultaneous localization and map building (SLAM) problem," *IEEE Trans. Robot. Autom.*, vol. 17, no. 3, pp. 229–241, 2001.

[14] G. P. Huang, A. I. Mourikis, and S. I. Roumeliotis, "A quadratic-complexity observability-constrained unscented Kalman filter for SLAM," *IEEE Trans. Robot.*, vol. 29, no. 5, pp. 1226–1243, Oct. 2013.

[15] J. Sola, A. Monin, M. Devy, and T. Vidal-Calleja, "Fusing monocular information in multicamera SLAM," *IEEE Trans. Robot.*, vol. 24, no. 5, pp. 958–968, Oct. 2008.

[16] J. A. Hesch, D. G. Kottas, S. L. Bowman, and S. I. Roumeliotis, "Consistency analysis and improvement of vision-aided inertial navigation," *IEEE Trans. Robot.*, vol. 30, no. 1, pp. 158–176, Feb. 2014.

[17] T. Lupton and S. Sukkarieh, "Visual-inertial-aided navigation for high-dynamic motion in built environments without initial conditions," *IEEE Trans. Robot.*, vol. 28, no. 1, pp. 61–76, Feb. 2012.

[18] M. Kaess, A. Ranganathan, and F. Dellaert, "iSAM: Incremental smoothing and mapping," *IEEE Trans. Robot.*, vol. 24, no. 6, pp. 1365–1378, Dec. 2008.

[19] M. Montemerlo, S. Thrun, D. Koller, and B. Wegbreit, "FastSLAM 2.0: An improved particle filtering algorithm for simultaneous localization and mapping that provably converges," in *Proc. Int. Joint Conf. Artif. Intell.*, 2003, pp. 1151–1156.

[20] G. Grisetti, C. Stachniss, and W. Burgard, "Improved techniques for grid mapping with rao-blackwellised particle filters," *IEEE Trans. Robot.*, vol. 23, no. 1, pp. 34–46, Feb. 2007.

[21] C. Harris, Z. Bell, E. Doucette, J. W. Curtis, and W. E. Dixon, "Target tracking in the presence of intermittent measurements by a sparsely distributed network of stationary cameras," in *Proc. Am. Control Conf.*, 2020.

[22] G. V. Chowdhary and E. N. Johnson, "Theory and flight-test validation of a concurrent-learning adaptive controller," *J. Guid. Control Dynam.*, vol. 34, no. 2, pp. 592–607, Mar. 2011.

[23] G. Chowdhary, T. Yucelen, M. Mühlegg, and E. N. Johnson, "Concurrent learning adaptive control of linear systems with exponentially convergent bounds," *Int. J. Adapt. Control Signal Process.*, vol. 27, no. 4, pp. 280–301, 2013.

[24] A. Parikh, R. Kamalapurkar, and W. E. Dixon, "Integral concurrent learning: Adaptive control with parameter convergence using finite excitation," *Int J Adapt Control Signal Process*, vol. 33, no. 12, pp. 1775–1787, Dec. 2019.

[25] H. Schaub and J. Junkins, *Analytical Mechanics of Space Systems*, AIAA, Ed. New York: AIAA Education Series, 2003.

[26] M. H. Stone, "The generalized weierstrass approximation theorem," *Math. Mag.*, vol. 21, no. 4, pp. 167–184, 1948.

[27] M. Krstic, I. Kanellakopoulos, and P. V. Kokotovic, *Nonlinear and Adaptive Control Design*. New York, NY, USA: John Wiley & Sons, 1995.

[28] W. E. Dixon, A. Behal, D. M. Dawson, and S. Nagarkatti, *Nonlinear Control of Engineering Systems: A Lyapunov-Based Approach*. Birkhauser: Boston, 2003.

[29] G. Chowdhary and E. Johnson, "A singular value maximizing data recording algorithm for concurrent learning," in *Proc. Am. Control Conf.*, 2011, pp. 3547–3552.

[30] H. K. Khalil, *Nonlinear Systems*, 3rd ed. Upper Saddle River, NJ: Prentice Hall, 2002.

[31] R. Kamalapurkar, B. Reish, G. Chowdhary, and W. E. Dixon, "Concurrent learning for parameter estimation using dynamic state-derivative estimators," *IEEE Trans. Autom. Control*, vol. 62, no. 7, pp. 3594–3601, July 2017.

BIOGRAPHICAL SKETCH

Christian G. Harris received a Bachelor of Science degree in Mechanical Engineering from the University of Florida in December 2017. During his undergraduate studies, Christian began volunteering in the Nonlinear Controls and Robotics group under the advisement of Dr. Warren E. Dixon, where he assisted in the development of robotic platforms for vision-based navigation experiments. In January 2018, Christian started his graduate studies at the University of Florida, and began investigating topics related to target tracking using multi-agent systems, intermittent sensing, switched systems, and network control. During this time, he participated in several internships sponsored by the Air Force Research Laboratory (AFRL) including the AFRL Scholars Program in 2019. In August 2020, he received a Master of Science degree in Mechanical Engineering from the University of Florida.